Synthesis and conformational preferences of peptides and proteins with cysteine sulfonic acid

SCHOLARONE™
Manuscripts

Synthesis and conformational preferences of peptides and proteins with cysteine sulfonic acid

Megh R. Bhatt and Neal J. Zondlo*

Department of Chemistry and Biochemistry

University of Delaware

Newark, DE 19716

United States

* To whom correspondence should be addressed. email: *zondlo@udel.edu*, phone: +1-302-831-0197.

Abstract

Cysteine sulfonic acid (Cys-SO$_3$H; cysteic acid) is an oxidative post-translational modification of cysteine, resulting from further oxidation from cysteine sulfinic acid (Cys-SO$_2$H). Cysteine sulfonic acid is considered an irreversible post-translational modification, which serves as a biomarker of oxidative stress that has resulted in oxidative damage to proteins. Cysteine sulfonic acid is anionic, as a sulfonate (Cys-SO$_3^-$; cysteate), in the ionization state that is almost exclusively present at physiological pH (pKa ~ –2). In order to understand protein structural changes that can occur upon oxidation to cysteine sulfonic acid, we analyzed its conformational preferences, using experimental methods, bioinformatics, and DFT-based computational analysis. Cysteine sulfonic acid was incorporated into model peptides for α-helix and polyproline II helix (PPII). Within peptides, oxidation of cysteine to the sulfonic acid proceeds rapidly and efficiently at room temperature in solution with methyltrioxorhenium (MeReO$_3$) and H$_2$O$_2$. Peptides containing cysteine sulfonic acid were also generated on solid phase using trityl-protected cysteine and oxidation with MeReO$_3$ and H$_2$O$_2$. Using methoxybenzyl (Mob)-protected cysteine, solid-phase oxidation with MeReO$_3$ and H$_2$O$_2$ generated the Mob sulfone precursor to Cys-SO$_2^-$ within fully synthesized peptides. These two solid-phase methods allow the synthesis of peptides containing either Cys-SO$_3^-$ or Cys-SO$_2^-$ in a practical manner, with no solution-phase synthesis required. Cys-SO$_3^-$ had low PPII propensity for PPII propagation, despite promoting a relatively compact conformation in ϕ. In contrast, in a PPII initiation model system, Cys-SO$_3^-$ promoted PPII relative to neutral Cys, with PPII initiation similar to Cys thiolate but less than Cys-SO$_2^-$ or Ala. In an α-helix model system, Cys-SO$_3^-$ promoted α-helix near the N-terminus, due to favorable helix dipole interactions and favorable α-helix capping via a sulfonate-amide side chain-main chain hydrogen bond. Across all peptides, the sulfonate side chain was significantly less ordered than that of the sulfinate. Analysis of Cys-SO$_3^-$ in the PDB revealed a very strong propensity for local (i/i or i/i+1) side chain-main chain sulfonate-amide hydrogen bonds for Cys-SO$_3^-$, with > 80% of Cys-SO$_3^-$ residues exhibiting these interactions. DFT calculations conducted to explore these conformational preferences indicated that side chain-main chain hydrogen bonds of the sulfonate with the intraresidue amide and/or with the i+1 amide were favorable. However, hydrogen bonds to water or to amides, as well as interactions with oxophilic metals, were weaker for the sulfonate than the sulfinate, due to lower charge density on the oxygens in the sulfonate.

Introduction

Cysteine oxidation renders cysteine a chemical chameleon, fundamentally changing its chemical nature through a rich array of oxidation and ionization states (Figure 1).[1-5] While cysteine as a thiolate (Cys-S⁻) is a particularly strong nucleophile, cysteine sulfenic acid (Cys-SOH) is an exceptional electrophile. Cysteine residues are also modified to glutathionylated disulfides (glutathionylation), structural disulfides, S-nitrosyl (S–NO, S-nitrosylation), S-sulhydryl (persulfide, S–SH), polysulfide, S-acyl, and thioether forms, with the S-nitrosyl form particularly prone to generation of thiyl radicals (Cys-S•; Cys-S–NO bond dissociation energy ~ 32 kcal mol⁻¹).[6] Cysteine sulfenic acid is transient and particularly susceptible to reaction as an electrophile with thiolates to generate disulfides, while the sulfenate (Cys-SO⁻) ionization state can react as a nucleophile with oxidants (e.g. H_2O_2 or HOCl) to generate the sulfinic acid. In contrast to the disulfides and to sulfenic acid forms, the sulfinic acid oxidation state (Cys-SO₂H; the predominant form at physiological pH is the sulfinate, Cys-SO₂⁻) is unreactive with thiols or thiolates. Oxidation to cysteine sulfinic acid is reversible, however, via ATP-dependent reduction by sulfiredoxin.[7,8] Sulfiredoxin was recently demonstrated to be critical to the redox regulation of numerous human proteins, indicating that the sulfinate oxidation state is commonly generated, particularly under conditions of oxidative stress.[9]

Further oxidation of the sulfinate leads to the sulfonic acid (Cys-SO₃H, also called cysteic acid), a post-translational modification called S-sulfonylation. No enzyme is known to reduce cysteine sulfonic acid within proteins. As such, cysteine sulfonic acid is considered a biomarker of irreversible protein oxidative damage.[10,11] Cysteine sulfonic acid exists essentially exclusively in the sulfonate ionization state (Cys-SO₃⁻, also called the cysteate) at physiological pH (pKa ~ – 2). Thus cysteine oxidation to the sulfonate results in the conversion of a mostly nonpolar,

neutral species (thiol) into a polar, sterically demanding anion (Figure 1c).

Cysteine sulfonic acid has been observed in proteins in numerous contexts. For example, in human zinc-copper superoxide dismutase (SOD1), a protein that is protective against oxidative damage and that is misfolded and/or aggregated in neurodegenerative disorders, including in the Lewy bodies present in amyotrophic lateral sclerosis (ALS), Cys111 is observed to be oxidized to the sulfonic acid in disease and aggregation models.[12-15] Cysteine sulfonic acid has also been observed or implicated in models of heart disease and diabetes,[16-18] in reperfusion after myocardial ischemia,[11] in voltage-dependent anion channel isoforms in the outer mitochondrial membrane,[19,20] in loss of function and aggregation of peroxiredoxins,[21-24] in inactivation phosphorylation-dependent prolyl isomerase Pin1 that is protective against Alzheimer's disease,[25] and in inactivation of matrix metalloprotease-7 (MMP-7) and alcohol dehydrogenase,[26] among other targets identified via mass spectrometry-based proteomics.[27-35]

We previously examined the conformational preferences of cysteine sulfinic acid.[36] The cysteine sulfinate is a particularly electron-rich side chain, as an overall anion which also has a lone pair on sulfur. Cysteine sulfinate exhibited especially favorable interactions with the protein backbone, both through its oxygens and via the sulfur lone pair (e.g. as a hydrogen bond between a lone pair and a backbone amide hydrogen, or as an $n{\rightarrow}\pi^*$ interaction between a lone pair and the backbone carbonyl). Due to the lengths of bonds to sulfur and the presence of multiple electron donors, cysteine sulfinate has the unique ability (compared to encoded amino acids, such as the superficially similar Asp) to exhibit simultaneous hydrogen bonds to both the intraresidue amide H and the amide H of the subsequent residue.

Notably, cysteine sulfonic acid lacks a lone pair on sulfur, in contrast to all other oxidation states of cysteine, causing it to be non-nucleophilic and non-Lewis basic on sulfur.

4

Cysteine sulfonate is also quite sterically demanding, comparable in size to neopentylglycine (Npg) (Figure 1d). Electronically, the sulfonate has three Lewis-basic oxygen atoms capable of hydrogen bonding to solvent and/or to hydrogen-bond donor groups in proteins.[37] Oxygen is also distinct from sulfur in its metal-binding preferences, such that oxidation of cysteine to the sulfonate leads to a change from a preference for soft metals (for sulfur ligands) to a greater preference for binding more oxophilic metals (for oxygen ligands), with the sulfonate binding metals in either a monodentate or a bidentate manner. The cysteine thiol is also capable of favorable S–H/π interactions with the π face of aromatic rings.[38] Collectively, these properties make the cysteine sulfonate dramatically distinct from cysteine thiol or thiolate. As such, oxidation of cysteine in a protein to the sulfonic acid could have significant consequences due to changes in sterics, electrostatics, conformational preferences, and/or metal binding at the side chain. Indeed, oxidation of the active-site cysteine of the tyrosine phosphatase PTP1B causes structural charges and induction of disorder, resulting in the specific targeting of the Cys-sulfonated form of this protein for degradation via the E3 ubiquitin ligase Cullin1.[39] Herein, we examine the inherent conformational preferences of cysteine sulfonate, via biophysical analysis in model peptides, bioinformatics analysis of the PDB, and computational chemistry approaches. In order to conduct this analysis, we also develop novel approaches to the oxoform-specific synthesis of peptides with cysteine sulfonate.

Results

Synthesis of peptides containing cysteine sulfonic acid. As cysteine sulfonic acid is the terminal oxidation state of cysteine, the standard approaches to its synthesis involve the use of strongly oxidizing conditions (e.g. concentrated H_2O_2, NaOCl, peroxynitrite, or H_2O_2 with

formic acid [generating performic acid]) on a peptide containing cysteine (Figure 2).[40-42] For example, polymers containing cysteine sulfonic acid, used as heparin mimics that have anti-coagulation properties, were synthesized using a solution of 30% H_2O_2 to globally oxidize the cysteine residues.[43] However, these approaches typically generate multiple oxidation products (Figure 2a), with the additional complication that the sulfinate and sulfonate are both anionic and only differ by a single oxygen atom, posing challenges both in yield and purification of a single cysteine oxoform.

For example, in our work to understand the structural effects of cysteine oxidation to the sulfinic acid and to develop fluorescent sensors of the oxidation to the sulfinate,[36,44,45] we observed that subjection of a peptide containing cysteine to oxidation with any of H_2O_2, NaOCl, or peroxynitrite yielded a mixture of products in various cysteine oxidation states, with the major product (usually the sulfinic acid, but the results were dependent on the local peptide sequence) typically obtained in less than 50% yield. In peptides that lack oxidation-sensitive functional groups, iron-oxo chemistry (generated *in situ* from Fe(II) and H_2O_2) has been employed in superstoichiometric quantities to generate the cysteine sulfonate (Figure 2d),[46] but this chemistry is potentially limiting in more complex peptides. Other recent methods for this transformation include the use of iron nanoparticles in refluxing MeCN or refluxing EtOH,[47] or oxone or $KBrO_3$ for extended reaction times (48-72 h).[48] All of these methods have substantial drawbacks, especially in the synthesis of larger peptides with a diverse array of functional groups.

Methyltrioxorhenium(VII) (MeReO$_3$, MTO) is a versatile strong oxidant, which can be used in catalytic amounts, via catalyst regeneration with H_2O_2.[49] MTO reacts with alkyl or aryl thiols or disulfides to generate the corresponding sulfonic acids at room temperature in high yields and short reaction times (10 min to 2 h) (Figure 2e).[50-54] While MTO also reacts with

methionine and unprotected tryptophan,[55] the sulfoxide of the former can be readily reduced back to methionine, and the latter could potentially have oxidation prevented by protection of the indole nitrogen. We previously used MTO to synthesize peptides with the sulfonic acid of phenylalanine, via either 4-mercaptophenylalanine or its disulfide (Figure 2f).[53] The fast, high-yielding nature of this reaction encouraged us to explore the use of MTO for oxidation of cysteine to cysteine sulfonic acid within peptides.

We examined both solution-phase and solid-phase oxidation for the synthesis of peptides with cysteine sulfonic acid, with initial experiments conducted via solution-phase oxidation. A peptide was synthesized with Cys in the guest position (X) of a model peptide context (Ac-GPPXPPGY-NH$_2$). Peptides from this series have previously been used to determine the propensities of all encoded amino amino acids for polyproline II helix (PPII), as well the effects post-translationally modifications and unnatural amino acids on PPII stability.[36,56-60] After purification, the peptide Ac-GPPCPPGY-NH$_2$ was then subjected to oxidation with MTO/H$_2$O$_2$ (Figure 3). This reaction cleanly and rapidly generated the peptide containing cysteine sulfonic acid, with high conversion and with no evidence of tyrosine oxidation (by MS or NMR).

To confirm the generality of this synthetic approach, we also examined the solution-phase oxidation of a Baldwin-type model Ala/Lys-rich peptide.[61] Peptides of this sequence have previously been employed to determine the α-helix propensities of all encoded amino acids, as well as those of post-translationally modified amino acids.[36,59,60,62-64] Oxidation with MTO/H$_2$O$_2$ proceeded cleanly to convert the cysteine thiol to the sulfonic acid (Figure 4). To our knowledge, these are the first examples of the synthesis of peptides containing cysteine sulfonic acid using MTO/H$_2$O$_2$.

While this solution-phase oxidation method is convenient for the synthesis of peptides

with cysteine sulfonic acid, it requires the initial purification of the peptide with cysteine, subsequent oxidation, and finally the purification of the peptide with cysteine sulfonic acid. We sought to develop an alternative approach that would allow the direct synthesis of peptides with cysteine sulfonic acid, without the intermediate need to isolate the unoxidized peptide. Therefore, we also explored a solid-phase peptide modification strategy.[53,65,66] We reasoned that oxidation of cysteine to the sulfonic acid could be effected readily on the solid phase using the trityl cysteine protecting group, which is the standard protecting group for cysteine in Fmoc solid-phase peptide synthesis.[67] A model peptide for the initiation of PPII helix (Ac-XPPGY-NH$_2$, X = Cys), with cysteine trityl-protected, was subjected to selective trityl deprotection with 1% TFA, followed by solid-phase oxidation using MTO/H$_2$O$_2$ (Figure 5). The resultant peptide was subjected to standard cleavage/deprotection and HPLC purification, which indicated that the peptide with cysteine sulfonic acid was the predominant species (Figure 5b). To further test this solid-phase cysteine oxidation method, the Baldwin-type α-helical model peptide with cysteine at residue 2 was subjected to solid-phase Cys deprotection and oxidation, followed by resin cleavage/side-chain deprotection and HPLC analysis (Figure 6). The resultant peptide had an HPLC chromatogram similar (other than retention times, due to the polarity differences at the cysteine side chain) to that of the same peptide that was not subjected to oxidation. These results indicate that the solid-phase oxidation method proceeds with high yield and specific conversion of cysteine directly to its sulfonic acid on solid phase.

Finally, we sought to compare the conformational preferences of cysteine sulfonic acid and cysteine sulfinic acid. We previously developed a method for the high-yield synthesis of peptides containing cysteine sulfinic acid using the commercially available methoxybenzyl (Mob)-protected Fmoc-cysteine.[44] In that work, the protected amino acid was oxidized in

solution to the sulfone, and then incorporated into peptides via standard solid-phase peptide synthesis. After resin cleavage and side chain deprotection, the peptide containing the cysteine Mob sulfone was then purified and subjected to strong-acid-mediated Mob deprotection. In conceiving of how to conduct this sequence more efficiently, we reasoned that oxidation of Mob-protected cysteine could also be conducted on a fully synthesized peptide on solid phase, removing the necessity for solution-phase synthesis and for purification of the Fmoc-protected cysteine Mob sulfone. Therefore, we synthesized a version of the Baldwin α-helical model peptide with Mob-protected cysteine at residue 2 (Figure 7). This peptide was then subjected to oxidization on solid phase with MTO/H_2O_2, which effectively oxidizes thioethers to sulfones.[55] Cleavage from resin and general side-chain deprotection yielded a peptide with the sulfone of Mob-protected cysteine (Figure 7a). Finally, subjection of this peptide to strong-acid Mob deprotection cleanly generated the peptide with cysteine sulfinic acid (Figure 7b). This approach represents an alternative, highly practical manner to generate peptides with cysteine sulfinic acid, using commercially available amino acids with no requirement for solution-phase small-molecule synthesis or purification of the Fmoc amino acids.

Analysis of the conformational preferences of cysteine sulfonic acid within model peptides. These peptides were then examined via circular dichroism (CD) and NMR spectroscopies to understand the conformational preferences of cysteine sulfonate, in comparison to cysteine thiol, cysteine thiolate, and cysteine sulfinate. Within the context of a model peptide for polyproline II helix, cysteine sulfonate exhibited low PPII propensity (Figure 8, Table 1), as determined by the CD via the mean residue ellipticity of the positive band with a maximum at ~ 228 nm.[68] Cysteine inherently exhibits very low PPII propensity.[56,69] The PPII propensity of cysteine sulfonate was somewhat greater than that of cysteine in either ionization state, but was

lower than that of the cysteine sulfinate. Interestingly, despite the low PPII propensity of the sulfonate by CD, NMR analysis of the peptide indicated that it has a small $^3J_{\alpha N}$, indicating a more compact conformation in ϕ that is globally consistent with higher PPII population (Table 2).[56,57,70-73] These data suggested the possibility that cysteine sulfonate might have different propensities for PPII initiation versus PPII propagation. PPII is promoted by $n{\rightarrow}\pi^*$ interactions between consecutive carbonyls.[74-76] As such, an intraresidue sulfonate-amide hydrogen bond might be expected to increase PPII by making the conjugated Pro–1 carbonyl a better electron-donor for $n{\rightarrow}\pi^*$ interactions between consecutive carbonyls (i.e. between the Pro–1 carbonyl and the Cys-SO_3^- carbonyl), thus promoting PPII in cysteine sulfonate and the subsequent proline.[57,73-75,77] However, this same interaction, by increasing the electron density at that Pro–1 carbonyl, would make that carbonyl a weaker electron acceptor for $n{\rightarrow}\pi^*$ interactions from the prior carbonyl, and thus reduce PPII population at the prior residues.[63] Therefore, the sulfonate-amide hydrogen bond was expected to promote the initiation of PPII, but to have confounding effects on the propagation of PPII.

In order to test the ability of cysteine sulfonate as an initiator of PPII, we tested a new model system for PPII initiation, Ac-**X**-PPGY-NH$_2$. Peptides with this context were synthesized, with X = Ala, Cys, Cys-SO_2^-, and Cys-SO_3^-. Peptides were analyzed by circular dichroism and NMR spectroscopy (Figure 9, Table 3, Table 4). The data indicated that both cysteine sulfinate and cysteine sulfonate substantially promoted PPII relative to neutral cysteine, in contrast to data in the PPII propagation propensity model peptide context. Notably, the cysteine thiolate also promoted PPII initiation. All anionic cysteine oxoforms examined exhibited higher PPII initiation propensities than neutral cysteine, with those PPII propensities approaching those of alanine, one of the best amino acids for PPII propensity.[56,69,72]

The propensities of these cysteine oxoforms for α-helicity, when located near the N-terminus of an α-helix, were similarly examined, via analysis of their CD and NMR spectra when incorporated at the second residue of the α-helix (Figure 10, Table 5, Table 6). These data indicate that cysteine sulfonate has a higher α-helix propensity here than neutral cysteine, and similar to that of the cysteine thiolate. However, cysteine sulfonate has a reduced α-helix propensity here than the cysteine sulfinate oxoform. Overall, these results are consistent with a favorable interaction of the anions with the α-helix macrodipole, resulting in stabilization similar to that observed previously for native (Asp⁻, Glu⁻, Cys-S⁻) and post-translationally modified (pSer^{2-}, pThr^{2-}, Cys-SO$_2^-$) anionic side chains.[36,62,63,78-80] As an additional possible stabilizing factor, side chain-main chain hydrogen bonding for anionic side chains in α-helical peptides can be identified by a downfield shift in that residue's amide hydrogen H^N. Via this NMR criterion and the differences in the CD data, the sulfinate appears to significantly stabilize the α-helix via side chain-main chain hydrogen bonding, which functions as an α-helix N-cap.[81] In contrast, the relatively larger $^3J_{\alpha N}$ at Cys-SO$_3^-$ corroborates[82] that the sulfonate is not directly promoting a compact conformation at this residue. Collectively, the data suggest that the interaction of the sulfonate anion with the δ$^+$ of the helix macrodipole is the primary reason for the increased α-helicity of Cys-SO$_3^-$ compared to neutral Cys.

Analysis of the NMR spectra of the cysteine oxoforms across all peptides (Figure 11, Figure 12, Table 2, Table 4, Table 6) indicated three key trends. First, proline-rich peptides with Cys-SO$_2^-$ and Cys-SO$_3^-$ exhibited smaller values of $^3J_{\alpha N}$ at the Cys than in equivalent peptides with the Cys thiol, indicating that these oxidized anionic derivatives induce conformations that are more compact in ϕ than is observed for Cys thiol.[82] The basic conditions (pH ≥ 8) required to generate the cysteine thiolate result in fast exchange of the amide protons, precluding similar

analysis of the $^3J_{\alpha N}$ of cysteine thiolate. Second, the chemical shift of the amide hydrogen of the cysteine derivative globally was considerably more downfield in the sulfinate than in the sulfonate, which suggests inherently stronger side chain-main chain hydrogen bonds for the sulfinate than for the sulfonate.

Finally, the diasastereotopic β hydrogens of these cysteine oxoforms were examined (Figure 12, Table 2, Table 4, Table 6). In all peptides, the diastereotopic cysteine sulfinate Hβ were distinct (large Δδ) and substantially upfield of those in Cys. In contrast, the diastereotopic cysteine sulfonate Hβ were indistinguishable in all peptides, and in addition were substantially downfield of those in Cys. These data indicate that Cys-SO$_2^-$ exhibits a high degree of ordering in its side chain (χ_1 and χ_2 torsion angles), which puts the two Hβ in distinct (rather than conformationally averaged) chemical environments. In contrast, Cys-SO$_3^-$ exhibits greater conformational heterogeneity in its side chain, rendering those Hβ chemically equivalent. The Hβ chemical shift effects (upfield for Cys-SO$_2^-$, downfield for Cys-SO$_3^-$) are consistent with the electronic properties of the sulfur. In the sulfinate, the sulfur is more electron-rich, with a lone pair on the sulfur as part of an overall anion. However, in the sulfonate, the sulfur is relatively electron-poor, with no lone pair and with 3 highly electronegative oxygen atoms attached, rendering the sulfonate an electron-withdrawing group (despite the overall negative charge) that shifts the β hydrogens downfield.

Bioinformatics analysis of cysteine sulfonate in the PDB. In order to further understand how cysteine oxidation to the sulfonic acid could result in changes in protein structure, we conducted analysis of cysteine sulfonate residues in the PDB. The structures of cysteine sulfonate were compared with those of cysteine and cysteine sulfinate, in order to identify differences in the conformational preferences of the cysteine oxoforms. For cysteine residues,

only non-modified cysteine residues which were not in a disulfide bond were considered. The sulfonate and sulfinate ionization states are expected to predominate in crystal structures for these oxidized forms of cysteine. In contrast, for cysteine, either the thiol and thiolate forms may be present, and these were not differentiated in this analysis due to the difficulty in determining the presence of hydrogens on sulfur in protein crystal structures. Because of the relatively lower frequency of cysteine sulfinate and cysteine sulfonate in the PDB compared to native Cys, significantly lower resolution limits and higher % sequence identity were used for the oxidized forms of Cys, which is a caveat to the following analysis. In addition, the observed conformational preferences will be further biased by solvent accessibility and/or oxidative susceptibility of the cysteine residues, with the observed oxidized forms of cysteine inherently more solvent-exposed than those of unmodified cysteine. Active site cysteine residues are also in general more reactive to oxidants,[5,12,83,84] and thus the data set on the oxidized cysteine residues has an additional bias toward active-site cysteines.

Keeping in mind these caveats, the Ramachandran plots of the cysteine oxoforms indicate (Figure 13, Table 7) that Cys-SO$_3^-$ exhibits a somewhat reduced likelihood to be present in β conformations compared to cysteine, with a concomitant increased likelihood of adopting PPII. α-Helix (α_R) frequencies are similar. In addition, Cys-SO$_3^-$ is substantially more likely to be observed on the right side of the Ramachandran plot, with a special preference for the normally strongly disfavored classical γ and/or right-handed PPII conformation (PPII$_R$). The conformational preferences were further analyzed by examining the ϕ, ψ, and χ_1 torsion angles individually (Figure 14, Table 8). These data reveal a substantial reduction in extended conformations in ϕ and a substantial increase both in $\phi \sim -70°$, in $\phi > 0°$, and in $\psi < -80°$. Similar trends were observed in Cys-SO$_2^-$. Finally, the sulfonate exhibited a significantly lower

frequency of conformations with the side chain in the $\chi_1 = g^-$ rotamer, with a resultant increase in frequency in the t rotamer. These χ_1 preferences could potentially reflect steric effects due to the size of the sulfonate group. However, surprisingly, there was no reduction in population with the g^+ rotamer, despite the largest steric effects being inherently present in the g^+ rotamer,[85-87] when the sulfonate is *gauche* to both the main-chain N and the main-chain carbonyl. This relatively high frequency of g^+ rotamer despite potential steric clashes with the sulfonate is likely due to the possibilities for side chain-main chain hydrogen bonding with this rotamer (see below).

Representative structures from the PDB were analyzed individually (Figure 15). In particular, cysteine sulfonate was observed to frequently function as an α-helix capping motif, with the sulfonate side chain hydrogen bonding to the intraresidue amide or to adjacent amides (Figure 15a-d). Notably, this type of interaction can occur with multiple geometries, consistent with NMR data that suggested conformational heterogeneity at Cys-SO_3^- within α-helical peptides. Side chain-main chain hydrogen bonds were also observed in turns (Figure 15e). In contrast, within β strands, side chain-main chain hydrogen bonds were often longer (weaker), and appear to directly compete with the hydrogen bonding patterns that stabilize β-sheets (Figure 15f). Cysteine sulfonate was also observed as a central residue in γ-turns (Figure 16). Here, an intraresidue side chain-main chain sulfonate-amide hydrogen bond could potentially strengthen the C_i=O•••H–N_{i+2} hydrogen bond of the γ-turn, with hydrogen bonding from the sulfonate to the intraresidue ($i+1$ residue) amide hydrogen increasing electron density on the C_i=O carbonyl.

The role of side chain-main chain hydrogen bonds or other noncovalent interactions was analyzed specifically in the PDB (Figure 17). The sulfonate was most likely to engage in a hydrogen bond with the intraresidue amide NH, with these hydrogen bonds observed in 58% of all Cys-SO_3^- residues (Figure 17a). Hydrogen bonds with the amide NH of the subsequent

residue were also observed in 40% of residues, although these were in general weaker (longer distances) (Figure 17b). Moreover, hydrogen bonds were observed to *both* the *i* and *i*+1 amides in 16% of structures. Overall, local (*i*/*i* or *i*/*i*+1) side chain–main chain sulfonate–amide hydrogen bonds were observed in 81% of all structures of Cys-SO$_3^-$. In addition, the sulfonate side chain was observed to commonly engage in longer-range hydrogen bonds with the side chains of residues near in space (for additional examples see ref. [37], who noted a special overrepresentation of Cys-SO$_3^-$ hydrogen bonds with Thr, Arg, and Gly residues, as well as the presence of ordered water molecules around the sulfonate).[88]

Potential *n*→π* interactions between an oxygen of the sulfonate side chain and the intraresidue carbonyl were also observed in 38% of the structures (Figure 17c), although relatively few structures had an O•••C=O distance < 3.0 Å that would be consistent with a strong intraresidue *n*→π* interaction. Finally, the presence of cysteine sulfonate at the central residue of a γ-turn (normal γ or inverse γ) was quantified based on the interresidue (*i*/*i*+2) carbonyl-amide hydrogen bond distances (Figure 17d), with one-quarter of all structures exhibiting the hydrogen bonding pattern of a γ-turn. Overall, compared with Cys-SO$_2^-$,[36] Cys-SO$_3^-$ exhibited a greater frequency of side chain-main chain hydrogen bonds with the same residue (*i*/*i* interactions) and with the subsequent residue (*i*/*i*+1), as well as a greater frequency of intraresidue *n*→π* interactions. The greater frequency of local interactions likely reflects in part the degeneracy in rotation about χ_2 for Cys-SO$_3^-$, which results in all three sulfonate oxygens being able to potentially interact locally. In contrast, for Cys-SO$_2^-$, the χ_2 rotamers are non-equivalent, as the sulfur lone pair of the sulfinate is distinct in interaction modes from the diastereotopic oxygens, as is observed, for example, in its strong preference for S:•••C=O *n*→π* interactions that are not possible with the sulfonate.

Computational analysis of the conformational preferences and noncovalent interactions of cysteine sulfonate. The experimental and bioinformatics data on peptides and proteins with cysteine sulfonic acid suggested that sulfonate-amide side chain-main chain interactions significantly impact the conformational preferences of $CysSO_3^-$, including favoring less common regions of the Ramachandran plot. To explore how interactions of the backbone with the sulfonate could impact the conformational preferences of $CysSO_3^-$, we conducted computational investigations on the model molecule Ac-$CysSO_3^-$-NHMe. Geometry optimization calculations were conducted by DFT methods (M06-2X functional, 6-311++G(2d,2p) basis set, in implicit water) on a series of combinations of ϕ, ψ, and χ_1, in order to identify conformations that are favored, disfavored, and/or promote specific noncovalent interactions.[89,90] From the final geometry-optimized structures, the energies were determined by the MP2 method with the 6-311++G(2d,2p) basis set in implicit water.[91] Note that the energies reflect both the conformational energies and the presence of intramolecular hydrogen bonds and other intramolecular noncovalent interactions, but do not include the energies of potential hydrogen bonds with solvent (or interactions with solvent that are lost due to intramolecular hydrogen bonds). As such, intramolecularly hydrogen-bonded structures inherently appear to be lower in energy by these methods, and all calculated energies need to be considered within this context.

Geometry optimization calculations indicated that multiple structures with intraresidue or interresidue side chain-main chain hydrogen bonds are favorable (Figure 18). These hydrogen-bonded structures are observed in α-helical (α_R/δ) or PPII conformations with g^- or g^+ rotamers (all with intraresidue hydrogen bonds); in β/extended, PPII, or PPII$_R$ conformations with a *t* rotamer (each with an *i*/*i*+1 hydrogen bond); and in the inverse γ conformation with the g^- rotamer. In addition, dual hydrogen bonds between different oxygens of the sulfonate and both

the intraresidue (*i*) and subsequent-residue (*i*+1) amides were observed in the cluster I conformation[92,93] (ϕ,ψ = −104˚, −133˚) that is normally sparsely populated, but is an energy minimum for both Cys-SO$_3^-$- and Cys-SO$_2^-$.[36] In addition, side chain-main chain $n{\rightarrow}\pi^*$ interactions were observed with the sulfonate as an electron donor in the β, γ, and α$_L$ conformations.

Overall, the lowest energy conformation had the sulfonate in the sterically disfavored g^+ rotamer in the α$_R$/δ conformation. This conformation had an intraresidue hydrogen bond that was among the shortest hydrogen bonds observed. This conformation would be favorable both for nucleating α-helix formation (see also below) and for stabilizing type I or type II' β-turns. More broadly analyzing rotamer preferences as a function of main chain conformation, the *t* rotamer was associated with hydrogen bonds to the subsequent-residue amide hydrogen, and these hydrogen bonds were in general longer than hydrogen bonds to the intraresidue amide, consistent with bioinformatics data (Figure 17). The β conformation was also associated with longer hydrogen bonds, suggesting that side chain-main chain hydrogen bonds should disfavor the extended conformation.

In general, the conformational preferences identified via DFT calculations were consistent with the structures observed in the PDB representing inherent energy minima of cysteine sulfonate. In comparison with our prior analysis of the conformational preferences of cysteine sulfinic acid,[36] however, the preferences of Cys-SO$_3^-$ appeared less distinct, with longer hydrogen bonds and longer $n{\rightarrow}\pi^*$ interactions in the sulfonates than in the sulfinates. Therefore, we used the model compounds methyl sulfonate and methyl sulfinate to examine hydrogen bond strengths of sulfonates versus sulfinates, either to an amide or to water (Figure 19). Geometry optimization calculations followed by energy analysis indicated that the sulfinate exhibits closer

and stronger hydrogen bonds both to an amide and to water, compared to the sulfonate. These results are consistent with the significantly greater negative charge density on the oxygens of the sulfinate (formally $-1/2$) compared to the sulfonate (formally $-1/3$). These qualitative trends of charge density were confirmed by calculations using the CM5 method to determine partial charges on atoms, which indicated more δ^- on the oxygens of the cysteine side chain in Ac-CysSO$_2^-$-NHMe (-0.57) than in Ac-CysSO$_3^-$-NHMe (-0.50), as well as more δ^+ on the sulfur in Ac-CysSO$_3^-$-NHMe ($+0.48$) than Ac-CysSO$_2^-$-NHMe ($+0.21$) (Figure 19c). These calculations thus indicate greater anionic charge density on the oxygens in the sulfinate, and a greater electron-withdrawing effect of the sulfonate at Cβ. These results are also consistent with the substantially stronger inherent conformational preferences observed for cysteine sulfinate compared to the sulfonate. Notably, for both the sulfinate and the sulfonate, the anion-amide interaction was stronger than the anion-water interaction (by 0.7–0.8 kcal mol^{-1}). In contrast, water-water and water-amide hydrogen bonds are similar in strength (-4.0 kcal mol^{-1}) at this level of theory. These results suggest that sulfinate-amide and sulfonate-amide interactions should be observed preferentially compared to interactions with water, consistent with the very high frequency of side chain-main chain hydrogen bonds observed for these PTMs in the PDB (Figure 17).

In addition, we examined the binding of methyl sulfinate and methyl sulfonate to the oxophilic metal Mg^{2+}. These calculations revealed substantially stronger metal binding for the sulfinate compared to the sulfonate (Figure 19d). We previously designed terbium-binding peptides that are specific sensors of the cysteine sulfinate oxoform Cys-SO$_2^-$ over the Cys-SH/Cys-S$^-$, Cys-SNO, Cys-SSGlutathione, and Cys-SO$_3^-$ oxoforms, with exceptional specificity for binding the sulfinate over the sulfonate.[45] These calculations confirm the significantly greater

affinity of the sulfinate for certain oxophilic metals compared to the sulfonate, again likely due to differences in oxygen charge density.

Finally, we computationally examined the conformational preferences of $Cys-SO_3^-$ within the context of a proline-rich peptide and within an α-helical peptide, in order to provide further insights into the experimental data. Within an $Ac-PP-CysSO_3^--PP-NMe_2$ context, we found that the g^- or g^+ rotamers were preferred for PPII, with the PPII conformation in each stabilized by a sulfonate-amide side chain-main chain hydrogen bond (Figure 20). These structures differed substantially in the main chain torsion angles both at $Cys-SO_3^-$ and at the subsequent proline, with the lower-energy g^- rotamer promoting a more compact conformation at $Cys-SO_3^-$ and a more canonical PPII conformation at Pro4. In contrast, in the t rotamer, a steric clash between the sulfonate and proline caused more distorted PPII conformations at both residues, as well as a non-ideal χ_1 torsion angle ($-151°$ observed, versus $\pm180°$ canonical). These results are consistent with the modest PPII propensity of $Cys-SO_3^-$, with the generally favored t χ_1 rotamer (Figure 14, Table 8) being unfavorable for PPII.

We also computationally examined the conformational preferences of Cys-SH, $Cys-S^-$, $Cys-SO_2^-$, and $Cys-SO_3^-$ in a model α-helical peptide context (Figure 21). Cysteine in the thiol form exhibited modest rotamer preferences, due to the absence of favorable side chain-main chain hydrogen bonds, consistent with prior bioinformatics data.[85,86] In contrast, in the g^- and g^+ rotamers, the Cys thiolate $Cys-S^-$ exhibited both side chain-main chain hydrogen bonds and a large reduction in the overall dipole moment (due to the favorable interaction of the anion with the helix macrodipole)[94], consistent with CD data showing significantly greater α-helicity in the thiolate ionization state. Similarly, the side chain-main chain hydrogen bond and large reduction in the overall dipole moment due to anion-helix macrodipole interactions were rotamer

dependent for both Cys-SO$_2^-$ and Cys-SO$_3^-$, with the largest effects in the g^- and g^+ rotamers. The sulfinate exhibited closer hydrogen bonds than the sulfonate in both the g^- and g^+ rotamers. The t rotamer, which lacked a side chain-main chain hydrogen bond, was substantially higher in energy and had a significantly larger overall dipole moment. Collectively, these computational results indicate that both cysteine sulfonate and cysteine sulfinate can stabilize α-helices at their N-termini through a combination of favorable side chain-main chain hydrogen bonds to the normally solvent-exposed amide hydrogens at the N-terminus of an α-helix, and through favorable interactions of the anionic side chain with the large macrodipole inherent to α-helices.

Discussion

Herein, we sought to examine how oxidation of cysteine to the sulfonic acid has the potential to change structure in proteins. In addition, we developed new methods for the oxoform-specific synthesis of peptides with cysteine sulfonate.

Synthesis of peptides with cysteine sulfonic acid. We developed a new method for the synthesis of peptides containing cysteine sulfonic acid. Using MeReO$_3$ (MTO) with H$_2$O$_2$, peptides containing cysteine sulfonic acid were synthesized rapidly and with high conversion, with minimal amounts of side products that are in an intermediate oxidation state. This method was demonstrated to be highly effective both in solution phase and (using trityl-protected Cys) on protected peptides on the solid phase. The method was specifically compatible with tyrosine, although it is likely incompatible with methionine or unprotected tryptophan. Based on the observed clean oxidation of thioethers using MTO on solid phase, we also applied MTO/H$_2$O$_2$ to synthesize peptides containing cysteine sulfinic acid via oxidation on the solid phase, via oxidation of Mob-protected Cys to generate the sulfone and subsequent Mob deprotection under

strongly acidic conditions. The combination of these approaches allows the ready synthesis of peptides containing Cys in high yield in one specific cysteine oxoform, as either the sulfinic acid (using Mob-protected Cys) or the sulfonic acid (using trityl-protected Cys), with both approaches employing commercially available side chain-protected forms of Fmoc-cysteine.

Structural effects of cysteine oxidation to cysteine sulfonic acid. The conformational preferences of cysteine sulfonate were examined in solution, using model peptides to test PPII propagation, PPII initiation, and α-helicity. Cysteine in the neutral thiol form has low PPII and α-helix propensities in all model system contexts examined.[56,62,69] The sulfonate exhibits only modestly greater propensity for PPII propagation than Cys, despite promoting a more compact ϕ. In contrast, cysteine sulfonate more effectively initiates PPII, potentially due to an intraresidue sulfonate-amide hydrogen bond promoting an interresidue $n{\rightarrow}\pi^*$ interaction that favors PPII (Figure 18def, Figure 19). That same interaction would make the carbonyl of the prior residue a weaker acceptor for an $n{\rightarrow}\pi^*$ interaction, and thus lead to lower PPII populations on residues prior to Cys-SO$_3^-$. This dichotomy of effects of a sulfonate-amide hydrogen bond explains the difference in the PPII propagation versus PPII initiation propensities of cysteine sulfonate.

Oxidation of cysteine to the sulfonate increases α-helicity at the N-terminus of α-helices via two effects: hydrogen bonding of the sulfonate to amide hydrogen(s) that are otherwise not involved in stabilizing the α-helix (helix capping), and via a substantial reduction of the (energetically unfavorable) α-helix macrodipole. Both of these effects are rotamer-dependent, occurring via the g^- or g^+ rotamers, but not the t rotamer.

Bioinformatics analysis of cysteine sulfonate in the PDB, with comparison to Cys, indicated a modestly lower frequency of cysteine sulfonate in β/extended conformations, and a modestly higher frequency on the right side of the Ramachandran plot. Importantly, these effects

are likely due to a combination of (1) the inherent conformational preferences of cysteine sulfonate and (2) solvent accessibility, whereby residues in turns and loops are more solvent-exposed than those in the interiors of proteins, and thus residues in loops and turns are more likely to be oxidized than those in (typically more buried) β-sheets. With this caveat, bioinformatics data indicate a change in the χ_1 rotamer preferences for Cys-SO$_3^-$ compared to Cys, with a higher preference for the *t* rotamer and a lower preference for the g^- rotamer for Cys-SO$_3^-$. The reduced preference for the g^- rotamer is potentially due to steric effects, due to the sulfonate group being similar in size to a *tert*-butyl group (Figure 1d).

In contrast to neutral cysteine, cysteine sulfonate only has hydrogen-bond acceptor groups. The sulfonate was observed to engage with high frequency in hydrogen bonds with the amide of the same residue (via the g^- or g^+ rotamers) or with the amide of the subsequent residue (via the *t* rotamer). In addition, two of the sulfonate oxygens can simultaneously interact with both the intraresidue amide hydrogen and the following-residue amide hydrogen, which promotes an unusual conformation with $(\phi, \psi) \sim (-100°, -130°)$. This conformation was termed the cluster I conformation by Balaram and by Chakrabarti in analyses of structures in the "disallowed" regions of the Ramachandran plot.[92,93] A similar dual-hydrogen bonded structure was previously observed for cysteine sulfinate.[36] The ability of these cysteine oxoforms to engage in dual hydrogen bonds with both the *i* and *i*+1 residue amides is dependent both on the presence of multiple oxygens and on the long S–O bond lengths.

Overall, side chain interactions of cysteine sulfonate were weaker (e.g. as observed in longer hydrogen bond lengths) than those of cysteine sulfinate, presumably primarily due to the lower charge density on the oxygens in the sulfonate. However, Cys-SO$_3^-$ has an entropic advantage in interactions compared to Cys-SO$_2^-$. In the sulfinate, due to the presence of one lone

22

pair plus two diastereotopic oxygens on the sulfur, there are three low-energy conformations about the χ_2 torsion angle. In contrast, in the sulfonate, the three oxygens are equivalent, and as such the energy minima via rotation at χ_2 are degenerate. This entropic advantage of the sulfonate likely partially counteracts the enthalpic advantage of the sulfinate in hydrogen bonding, explaining the similarities of their conformational preferences in model peptides despite the weaker backbone interactions for the sulfonate, as well as the very high frequency of local sulfonate-amide hydrogen bonds.

Cysteine oxidation to the sulfonate form introduces three oxygens that are Lewis basic and capable of serving as hydrogen bond acceptors, generating substantially greater steric bulk and, at physiological pH, a fixed overall negative charge. As neutral cysteine is a relatively nonpolar amino acid, these modifications have the potential to dramatically impact local interactions and structure at an oxidized cysteine. The work herein provides a context for understanding structural and functional changes of oxidation of cysteine to cysteine sulfonic acid within proteins.

Methods

Peptide synthesis. Standard peptide synthesis, purification, and characterization are described in the Supporting Information.

Cysteine oxidation to cysteine sulfonic acid within peptides. Cysteine was oxidized to the sulfonic acid oxoform by two methods. ***Solution-phase oxidation***. The solution-phase synthesis of peptides containing cysteine sulfonic acid was achieved by oxidation of a purified peptide containing Cys using 1 M H_2O_2 and 1.2 mM methyltrioxorhenium (MTO) in CH_3CN. The excess H_2O_2 was quenched with dithiothreitol (DTT) and the reaction mixture was filtered

and purified via analytical HPLC. Additional details are in the Supporting Information. ***Solid-phase oxidation***. Peptides containing trityl-protected cysteine were synthesized via solid-phase peptide synthesis. The trityl group was selectively removed using 1% TFA with 5% triisopropylsilane (TIS) in CH_2Cl_2. The resin was washed and subjected to oxidation with 0.3 M H_2O_2 and 0.4 mM methyltrioxorhenium (MTO) in $CH_3CN:CH_2Cl_2$ 1:1 on the solid phase to produce the peptides containing cysteine sulfonic acid. The peptides were subjected to cleavage from the resin and deprotection using 95% TFA/5% TIS, then purified via analytical HPLC. The obtained peptides were analyzed and confirmed via ESI mass spectrometry and NMR spectroscopy. Additional details are in the Supporting Information.

Solid-phase cysteine oxidation to cysteine sulfinic acid. Peptides were synthesized on Rink amide resin by incorporating Fmoc-Cys(Mob)-OH at site to be oxidized. After the synthesis of the unmodified peptide was completed, the resin was washed with CH_2Cl_2 and DMF. A mixture of 0.3 M H_2O_2 and 0.4 mM methyltrioxorhenium (MTO) in $CH_3CN:CH_2Cl_2$ 1:1 was added. The reaction was allowed to proceed for 2 hours, then the resin was washed with DMF and CH_2Cl_2, then dried with ether. The peptides were then subjected to cleavage from the resin and protecting groups other than Mob were removed using 95% TFA/5% TIS. The peptides were purified using HPLC, lyophilized overnight, and the Mob group deprotection was effected using 50% TfOH/45% TFA/5% H_2O. The resultant peptides containing cysteine sulfinic acid were purified via HPLC. Additional details are in the Supporting Information.

Circular dichroism. CD experiments were performed on a Jasco spectropolarimeter using a 1 mm cell, at 0.5 ˚C or 25 ˚C and peptide concentrations of 50-150 μM in 5 mM phosphate buffer (at pH 4.0, 7.0, or 8.5) containing 25 mM KF. The data are the average of at least three independent trials, with data collected every nm, an averaging time of 8 s and at least

three accumulations. Peptide concentrations were determined by UV-Vis spectroscopy. Data are background corrected but are not smoothed. Additional details are in the Supporting Information.

NMR spectroscopy. NMR spectra of the peptides were recorded at the temperatures indicated on a Brüker 400 or 600 MHz NMR spectrometer using a triple-resonance cryoprobe or a TXI probe. The peptides were allowed to dissolve in 5 mM phosphate buffer (pH 4 or as indicated) with 25 mM NaCl and 100 μM TSP in 90% H_2O/10% D_2O, and the pH was adjusted as needed. 1-D NMR spectra were obtained using an excitation sculpting pulse sequence. TOCSY NMR spectra were collected using an excitation sculpting TOCSY pulse sequence, with sweep widths of 12.25 ppm in t_1 and t_2, 512×1024 complex data points, 8 scans per t_1 increment, a relaxation delay of 1.7 s, and a TOCSY mixing time of 80 ms. All resonances were calibrated with respect to TSP, which was referenced at 0.00 ppm. The data were processed in MestReNova and Sparky. Additional details are in the Supporting Information.

Bioinformatics. On April 11, 2022, a search of the Protein Data Bank (PDB) was conducted for structures containing cysteine sulfonic acid (chemical ID OCS), cysteine sulfinic acid (chemical ID CSD), and non-disulfide and unmodified cysteine (chemical ID CYS) residues within a protein polymer. A total of 282, 487, and 1,038,729 structures were found, respectively, and were filtered using the advanced filter option on the RCSB website. These structures were filtered based on resolution with a threshold of 3.0 Å for OCS and CSD and 1.1 Å for CYS. These structures were also filtered based on sequence identity, with a threshold of 90% for OCS, 90% for CSD, and 30% for CYS. Only unique chains from these structures were included in the data set. After the filtration process, 141, 216, and 431 PDB structures were obtained, containing 146, 226, and 1460 OCS, CSD, and CYS residues, respectively. Perl scripts were written and applied to extract or calculate relevant information including residue number and identity,

interatomic angles, and distances. Additional details are in the Supporting Information.

Computational chemistry. All calculations were conducted with Gaussian 09.[95] Geometry optimization calculations on Ac-CysSO$_3^-$-NHMe were conducted via iterative optimization methods, with the final geometry optimization calculations conducted using the M06-2X DFT functional and the 6-311++G(2d,2p) basis set in implicit water (IEFPCM method).[89,90,96] All final geometry-optimized structures were subjected to frequency calculations using the same functional and basis set, which indicated zero negative (imaginary) frequencies. The electronic energies of these structures were then determined using the MP2 method with the 6-311++G(2d,2p) basis set in implicit water (IEFPCM).[91]

Small-molecule structures of methyl sulfonate and methyl sulfinate, either free or bound to H$_2$O, to methyl acetamide (AcNHMe), or to Mg^{2+}, were generated via iterative geometry optimization methods, with the final optimizations conducted using the M06-2X DFT functional and the aug-cc-pVTZ basis set in implicit water (IEFPCM).[97] All final geometry-optimized structures were then subjected to frequency calculations, which indicated zero negative (imaginary) frequencies. Interaction energies of these complexes were determined via component energy analysis, in which the interaction energy was determined by subtracting the energies of the individual geometry-optimized molecules from the energy of the complex, with all energy calculations conducted using the MP2 method and the aug-cc-pVQZ basis set in implicit water (IEFPCM). This large basis set was employed in order to minimize error due to basis set superposition error (BSSE).[98,99] Vacuum-based counterpoise calculations indicated that the BSSE was less than 10% of the total (aqueous) interaction energy for all complexes.

Geometry-optimized structures of Ac-PP-CysSO$_3^-$-PP-NMe$_2$, as a function of cysteine sulfonate χ_1 side-chain rotamer, in the PPII conformation at all residues and with the *exo* ring

pucker at all proline residues, were generated via iterative geometry optimization. The final geometry optimization calculations were conducted with the M06-2X DFT functional and the 6-31+G(d,p) basis set in implicit water (IEFPCM).

Geometry-optimized structures of Ac-Ala-CysX-Ala$_9$-NHMe, as a function of cysteine χ_1 side-chain rotamer and cysteine ionization and oxidation state, in the α-helix conformation at all residues, were generated via iterative geometry optimization from an initial Ac-Ala$_{11}$-NHMe model. All final models were generated using the M11-L DFT functional[100] and the Def2SVP basis set[101] in implicit water (IEFPCM model).

Coordinates of all geometry-optimized structures are in the Supporting Information.

Acknowledgements

Supporting Information Available

Full synthetic procedures and characterization of all peptides, full 1-D and TOCSY NMR spectra for peptides, additional analysis, and coordinates of all geometry-optimized structures. This material is available free of charge via the Internet at the journal web site.

Figures
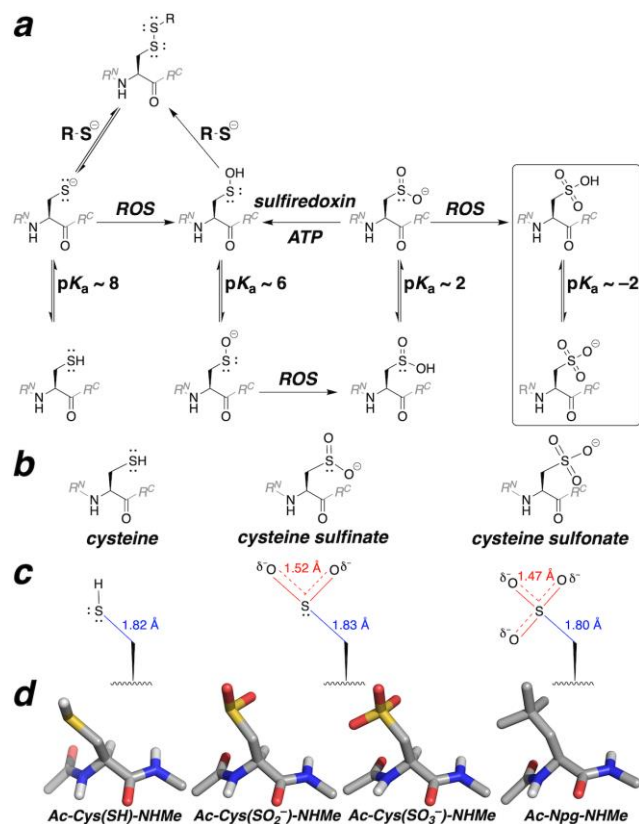
Figure 1. Major oxidative post-translational modifications of protein cysteine residues. (a) Oxidation and ionization states of cysteine that can be generated as a result of exposure to reactive oxygen species (ROS), including disulfide (Cys-S-S-Cys), thiol (Cys-SH)/thiolate (Cys-S⁻), sulfenic acid (Cys-SOH)/sulfenate (Cys-SO⁻), sulfinic acid (Cys-SO$_2$H)/sulfinate (Cys-SO$_2^-$), and sulfonic acid (Cys-SO$_3$H)/sulfonate (Cys-SO$_3^-$). R^N and R^C represent the N-terminal and C-terminal residues, respectively, to the cysteine. (b) The forms of cysteine, cysteine sulfinate, and cysteine sulfonate that predominate in proteins and peptides at physiological pH, showing the charges and lone pairs. (c) C–S and S–O bond lengths in cysteine, cysteine sulfinate, and cysteine sulfonate. (d) Minimal models of the cysteine oxoforms Ac-Cys(SH)-NHMe, Ac-Cys(SO$_2^-$)-NHMe, Ac-Cys(SO$_3^-$)-NHMe, and the sterically similar Ac-Npg-NHMe (Npg = neopentylglycine), providing a visual representation of the structural variations that occur in cysteine residues as a result of oxidation. The structures in (c) and (d) were generated based on restrained geometry optimization, with the ϕ and ψ angles fixed at –135º and +135º, respectively, using the M06-2X DFT functional and the aug-cc-pVTZ basis set in implicit H$_2$O. Restrained geometry optimization with this β conformation was employed to avoid changes in the geometries due to differences in side chain-main chain hydrogen bonding.
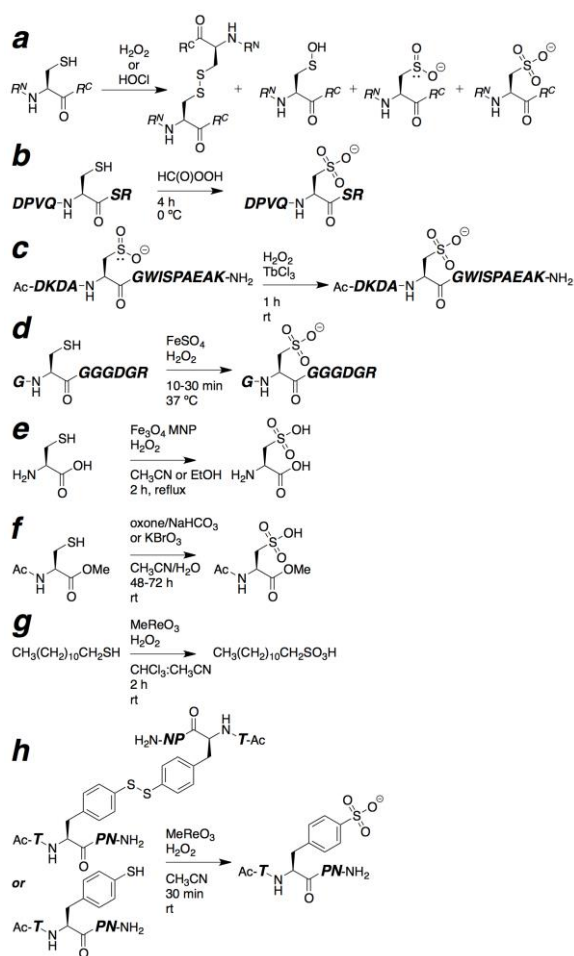
Figure 2. Methods to synthesize the sulfonic acid group in peptides containing cysteine and in other sulfur-containing compounds. (a) Oxidation of cysteine in a peptide using H_2O_2 or HOCl. (b) Oxidation of cysteine thiol to cysteine sulfonic acid using performic acid (synthesized *in situ* via 30% H_2O_2:HCOOH 1:19).[40-42] (c) Oxidation of cysteine sulfinic acid to the sulfonic acid with H_2O_2 catalyzed by TbCl$_3$. This approach, while compatible with Trp, requires the prior synthesis of the peptide with cysteine sulfinic acid, and likely also is dependent on the terbium-binding properties of the peptide oxidized.[45] (d) Conversion of cysteine thiol in a peptide to cysteine sulfonic acid, using H_2O_2 and FeSO$_4$.[46,102] (e) Conversion of Cys(SH) to Cys(SO$_3$H) using Fe$_3$O$_4$ magnetic nanoparticles (MNPs)/H_2O_2 in CH$_3$CN or EtOH.[47] (f) Oxidation of Ac-Cys(SH)-OMe to Ac-Cys(SO$_3$H)-OMe using oxone/NaHCO$_3$ or KBrO$_3$.[48] (g) Conversion of thiols to sulfonic acids using H_2O_2 and MeReO$_3$ (MTO). This method efficiently converts alkyl or aryl thiols or disulfides to the corresponding sulfonic acids at room temperature with high yields and short reaction times.[51,52] (h) The conversion of 4-mercaptophenylalanine or its disulfide in a peptide to sulfonic acid using H_2O_2 and MeReO$_3$.[53]
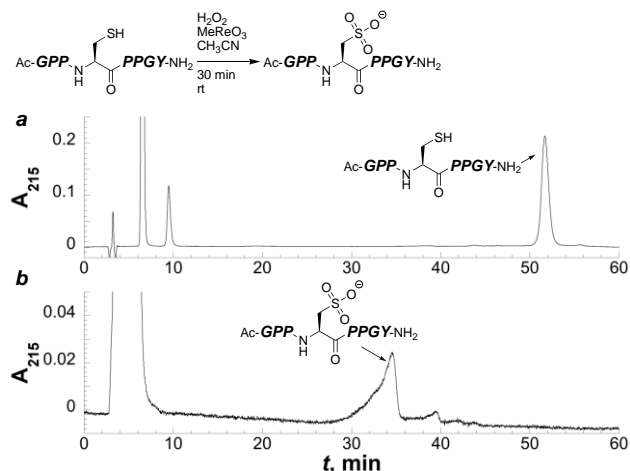
Figure 3. Solution-phase oxidation of a polyproline II helix model peptide with MeReO₃/H₂O₂. (a) HPLC chromatogram of a purified polyproline II helix propagation model peptide (Ac-GPPCPPGY-NH$_2$), prior to oxidation. (b) Crude HPLC chromatogram of the oxidation reaction mixture after 30 minutes, from a solution of ~500 µM peptide, 1 M H$_2$O$_2$, 1.2 mM MeReO$_3$ in CH$_3$CN, and ~0.1 M dithiothreitol (DTT). HPLC analysis was conducted using an analytical C18 column with a linear gradient of 0–25% buffer B (20% H$_2$O, 80% CH$_3$CN, and 0.05% TFA) in buffer A (98% H$_2$O, 2% CH$_3$CN, and 0.06% TFA) over 60 minutes. Peak broadening has previously been observed for peptides in the Ac-GPPXPPGY-NH$_2$ context, including in some peptides the presence of multiple peaks of the same molecular weight that are in equilibrium, apparently due to proline *cis-trans* isomerization at the four X-Pro amide bonds.[44,56,58,59]
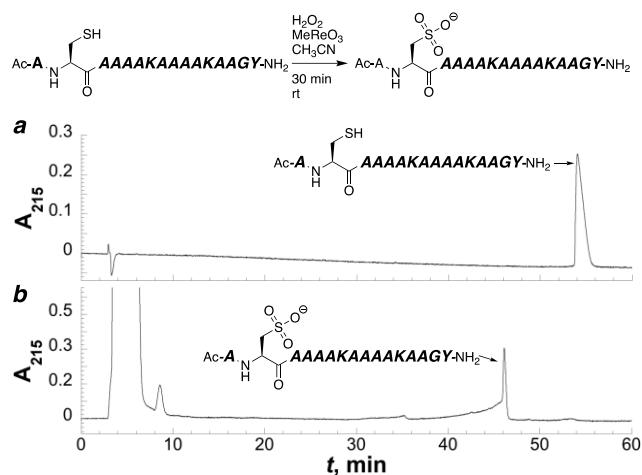
Figure 4. Solution-state oxidation of an α-helical model peptide with MeReO₃/H₂O₂. (a) HPLC chromatogram of the purified α-helical model peptide (Ac-ACAAAAKAAAAKAAGY-NH₂) prior to oxidation. (b) Crude HPLC chromatogram of ~50 μM peptide after being oxidized with 1 M H_2O_2 catalyzed by 1.2 mM MeReO₃ in CH₃CN at room temperature for 30 minutes, followed by quenching the reaction with 0.1 M dithiothreitol (DTT). HPLC analysis was conducted using an analytical C18 column with a linear gradient of 0–35% buffer B in buffer A over 60 minutes.
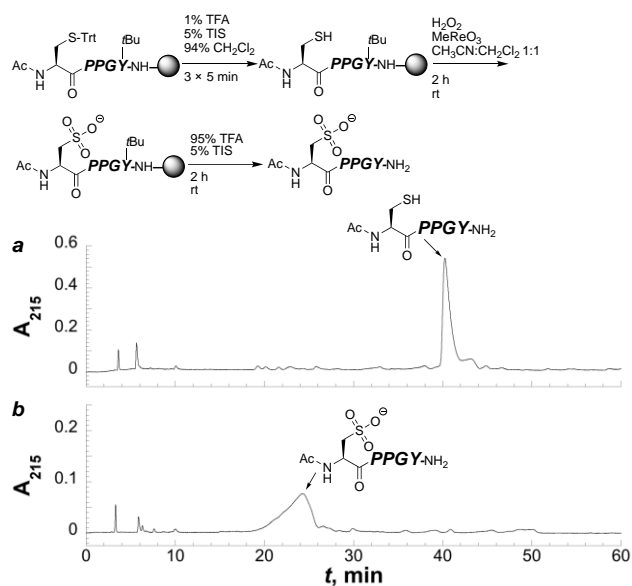
Figure 5. Solid-phase oxidation of peptide with MeReO₃/H₂O₂. (a) Crude HPLC chromatogram of the PPII initiation model peptide (Ac-CPPGY-NH₂) before oxidation, after cleavage from resin and deprotection. (b) Crude HPLC chromatogram of the peptide after oxidation on resin with 0.3 M H₂O₂ catalyzed by 0.4 mM MeReO₃ in CH₃CN:CH₂Cl₂ 1:1 for 2 hours at room temperature, followed by cleavage from resin and deprotection using 95% TFA/5% TIS for 2 hours at room temperature. HPLC analysis was conducted using an analytical C18 column with a linear gradient of 0–20% buffer B in buffer A over 60 minutes.
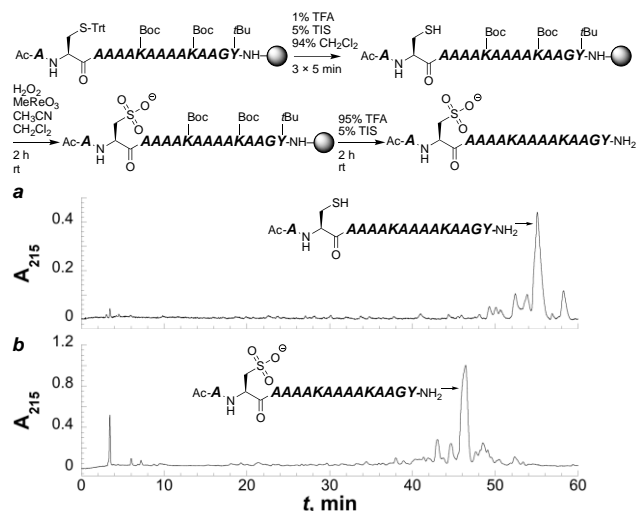
Figure 6. Oxidation of an α-helical model peptide with MeReO$_3$/H$_2$O$_2$ on solid phase. (a) Crude HPLC chromatogram of the α-helical model peptide Ac-ACAAAAKAAAAKAAGY-NH$_2$ prior to oxidation, after cleavage from resin and deprotection. (b) Crude HPLC chromatogram of the peptide after solid-phase oxidation with 0.3 M H$_2$O$_2$ catalyzed by 0.4 mM MeReO$_3$ in CH$_3$CN:CH$_2$Cl$_2$ 1:1 for 2 hours at room temperature, followed by cleavage from resin and deprotection with 95% TFA/5% TIS for 2 hours at room temperature. The oxidation reaction was preceded by selective removal of the trityl group on cysteine using 1% TFA/5% TIS in CH$_2$Cl$_2$. HPLC analysis was conducted using an analytical C18 column with a linear gradient of 0–35% buffer B in buffer A over 60 minutes.
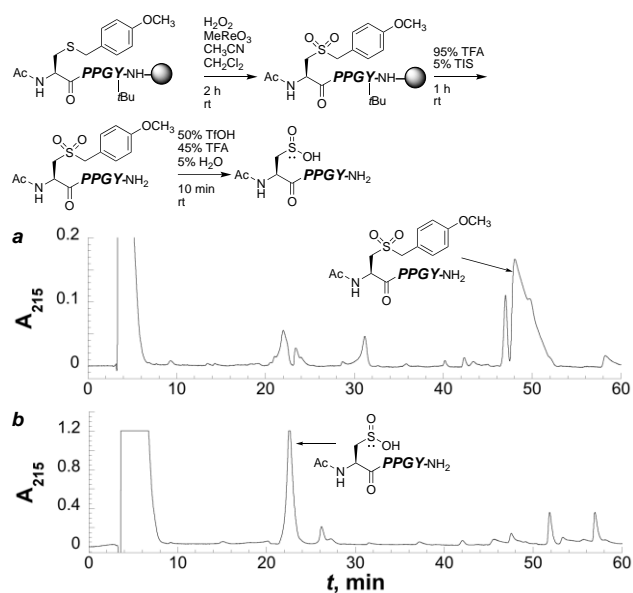
Figure 7. Oxidation of Mob-protected cysteine in a peptide with MeReO$_3$/H$_2$O$_2$ on solid phase to generate the peptide with cysteine sulfinic acid. (a) Crude HPLC chromatogram of the peptide after solid-phase oxidation with 0.3 M H$_2$O$_2$ catalyzed by 0.4 mM MeReO$_3$ in CH$_3$CN:CH$_2$Cl$_2$ 1:1 for 2 hours at room temperature, followed by cleavage from resin and deprotection of the *tert*-butyl (*t*Bu) protecting group on tyrosine using 95% TFA/5% TIS for 2 hours at room temperature. (b) Crude HPLC chromatogram of the purified peptide from (a) after deprotection of the 4-methoxybenzyl (Mob) group with 50% TfOH/45% TFA/5% H$_2$O for 10 minutes at room temperature. HPLC analysis was conducted using an analytical C18 column, in (a) with a linear gradient of 0–25% buffer B in buffer A over 60 minutes, or in (b) with a linear gradient of 0–20% buffer B in buffer A over 60 minutes.
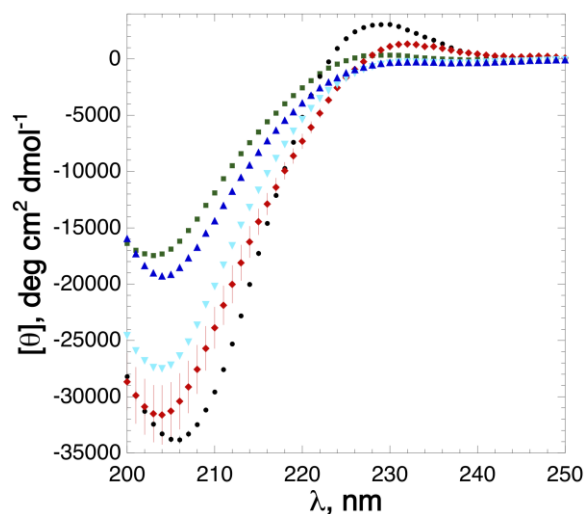
Figure 8. CD spectra of peptides with cysteine oxoforms in a model peptide of polyproline II helix (PPII) propagation. CD spectra of the peptides Ac-GPPXPPGY-NH$_2$, X = Cys-SO$_3^-$ pH 7 (green squares), Cys-SO$_2^-$ pH 7 (red diamonds), Cys-SH pH 4 (cyan inverted triangles), Cys-S$^-$ pH 8.5 (blue triangles), and Pro pH 7 (black circles). Spectra were acquired at the indicated pH in 5 mM phosphate buffer with 25 mM KF at 25 °C. To prevent cysteine oxidation during the experiment, spectra of peptides with unmodified cysteine were obtained in solutions with 0.1 mM TCEP. The data are the average of at least three independent trials, with error bars indicating standard error. The PPII helicity of the peptide is indicated by the magnitude of the local maximum (positive band) around 228 nm, with a larger (more positive) magnitude indicating a greater PPII population.
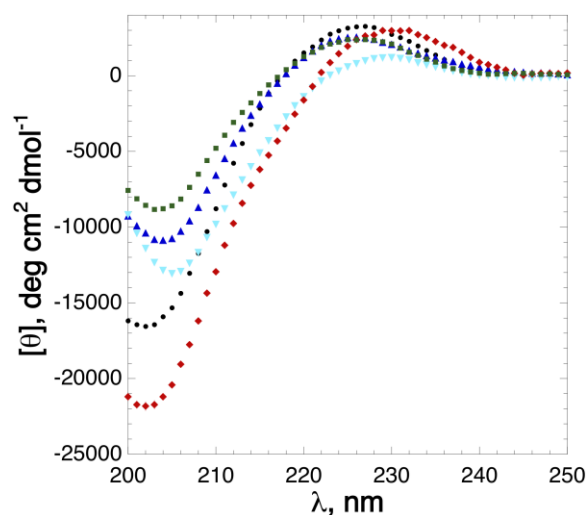
Figure 9. CD spectra of peptides with cysteine oxoforms in a model peptide of polyproline II helix (PPII) initiation. CD spectra of the peptides Ac-XPPGY-NH$_2$, where X = Cys-SO$_3^-$ at pH 7 (green squares), Cys-SO$_2^-$ at pH 7 (red diamonds), Cys-SH at pH 4 (cyan inverted triangles), Cys-S$^-$ at pH 8.5 (blue triangles), and Ala at pH 7 (black circles). The spectra of the peptides were obtained in a 5 mM phosphate buffer at the indicated pH containing 25 mM KF at 25 °C. The spectra of peptides with unmodified cysteine were obtained using a solution with 0.1 mM TCEP. The data are the average of at least three independent trials, with error bars representing standard error.
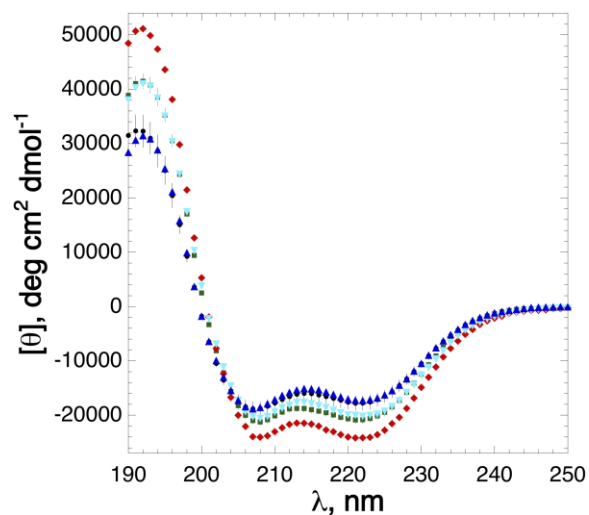
Figure 10. CD spectra of peptides with cysteine oxoforms in an α-helical model peptide. CD spectra of the peptides Ac-AXAAAAKAAAAKAAGY-NH$_2$, X = Cys-SO$_3^-$ pH 7 (green squares), Cys-SO$_2^-$ pH 7 (red diamonds), Cys-SH pH 4 (blue triangles), Cys-S$^-$ pH 8.5 (cyan inverted triangles), and Ala pH 4 (black circles). The spectra were acquired in 5 mM phosphate buffer at the indicated pH with 25 mM KF at 0.5 ºC. The spectra of peptides with unmodified cysteine were acquired with 0.1 mM TCEP in the solution. The data are the average of at least three independent trials, with error bars representing standard error.
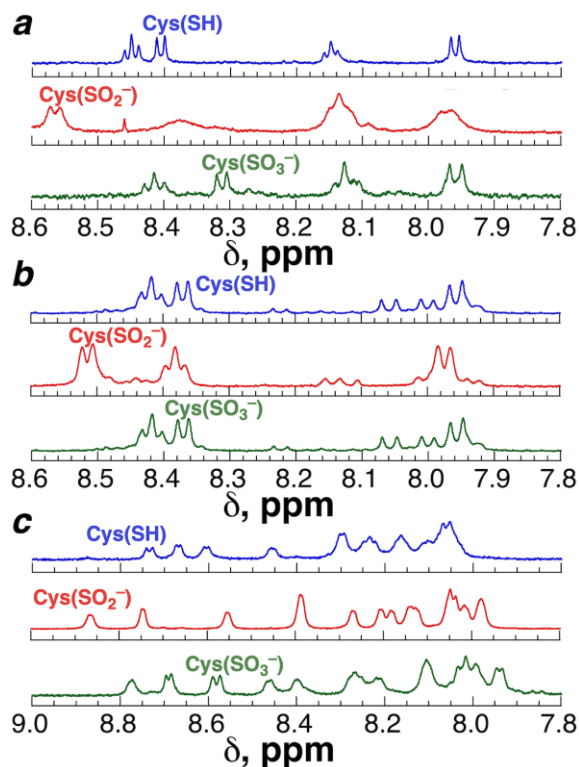
Figure 11. Amide regions of the ^{1}H NMR spectra of peptides containing cysteine sulfonate, cysteine sulfinate, and cysteine thiol. ^{1}H NMR spectra of the peptides (a) Ac-GPPXPPGY-NH$_2$, (b) Ac-XPPGY-NH$_2$, and (c) Ac-AXAAAAKAAAAKAAGY-NH$_2$ with the cysteine oxoforms X= Cys-SH (blue, top within each panel), Cys-SO$_2^-$ (red, middle of each panel), and Cys-SO$_3^-$ (green, bottom of each panel) for each of these peptides. NMR data were collected at pH 4 in 5 mM phosphate buffer with 25 mM NaCl and 90% H$_2$O/10% D$_2$O at (a, b) 300 K or (c) 274 K. Resonance assignments of cysteine oxoforms versus other resonances were determined via analysis of the fingerprint region of TOCSY spectra using standard approaches. See Figures S17-S31 for full details. Superpositions of the fingerprint regions of the TOCSY spectra in each sequence context, with annotation of the Cys oxoform resonances, are in Figure S21 (Ac-GPPXPPGY-NH$_2$), Figure S26 (Ac-XPPGY-NH$_2$), and Figure S31 (Ac-AXAAAAKAAAAKAAGY-NH$_2$).
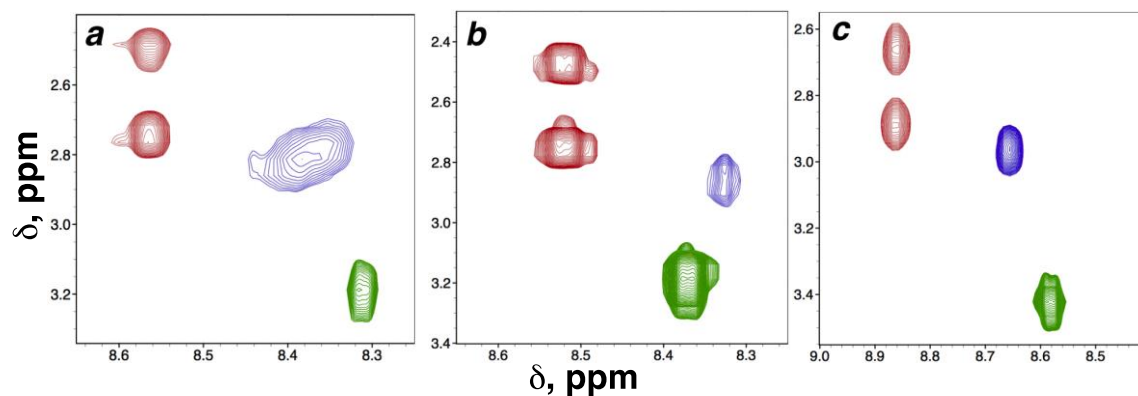
Figure 12. H^N-H$^\beta$ region of the TOCSY spectra of peptides containing cysteine sulfonate, cysteine sulfinate, and cysteine thiol. TOCSY NMR spectra of the peptides (a) Ac-GPPXPPGY-NH$_2$, (b) Ac-XPPGY-NH$_2$, and (c) Ac-AXAAAAKAAAAKAAGY-NH$_2$, with X= Cys-SH (blue), Cys-SO$_2^-$ (red), and Cys-SO$_3^-$ (green) in these peptides. Data were collected at pH 4 in 5 mM phosphate buffer with 25 mM NaCl and 90% H$_2$O/10% D$_2$O at temperatures of (a and b) 300 K or (c) 274 K. Full spectra are in the Supporting Information.
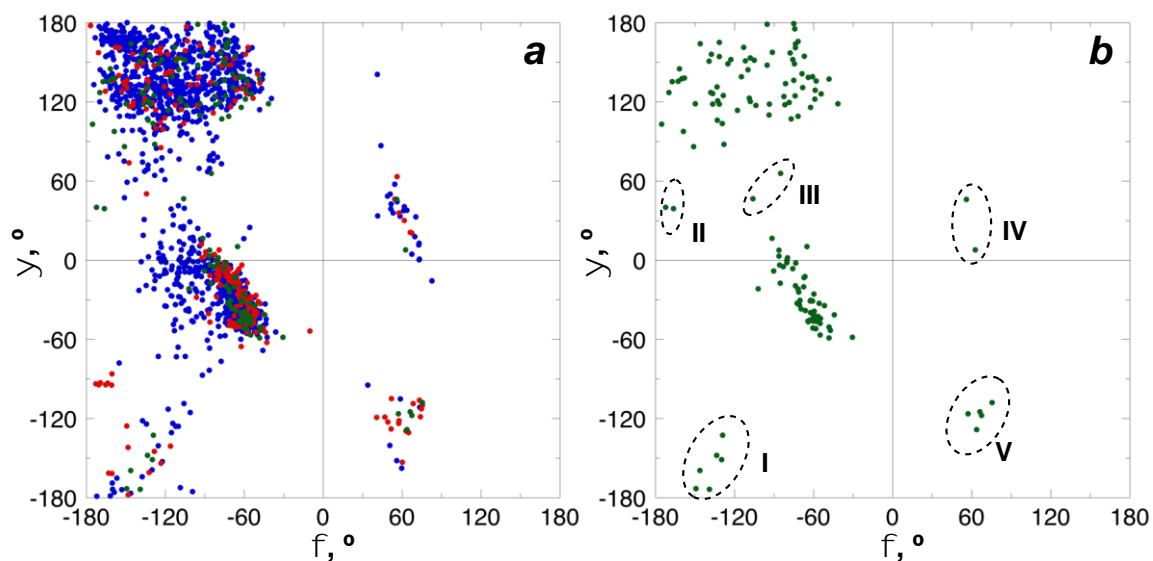
Figure 13. Ramachandran plots of cysteine, cysteine sulfinic acid, and cysteine sulfonic acid residues in the PDB. (a) Ramachandran plots of cysteine sulfonic acid (green), cysteine sulfinic acid (red), and cysteine (blue) residues in the PDB. (b) Ramachandran plot of cysteine sulfonic acid residues. Summaries of these data are in Table 7. Individual Ramachandran plots for cysteine and cysteine sulfinic acid are in the Supporting Information. The Roman numerals in (b) represent unique structures, which are shown in Figure S33 in the Supporting Information.
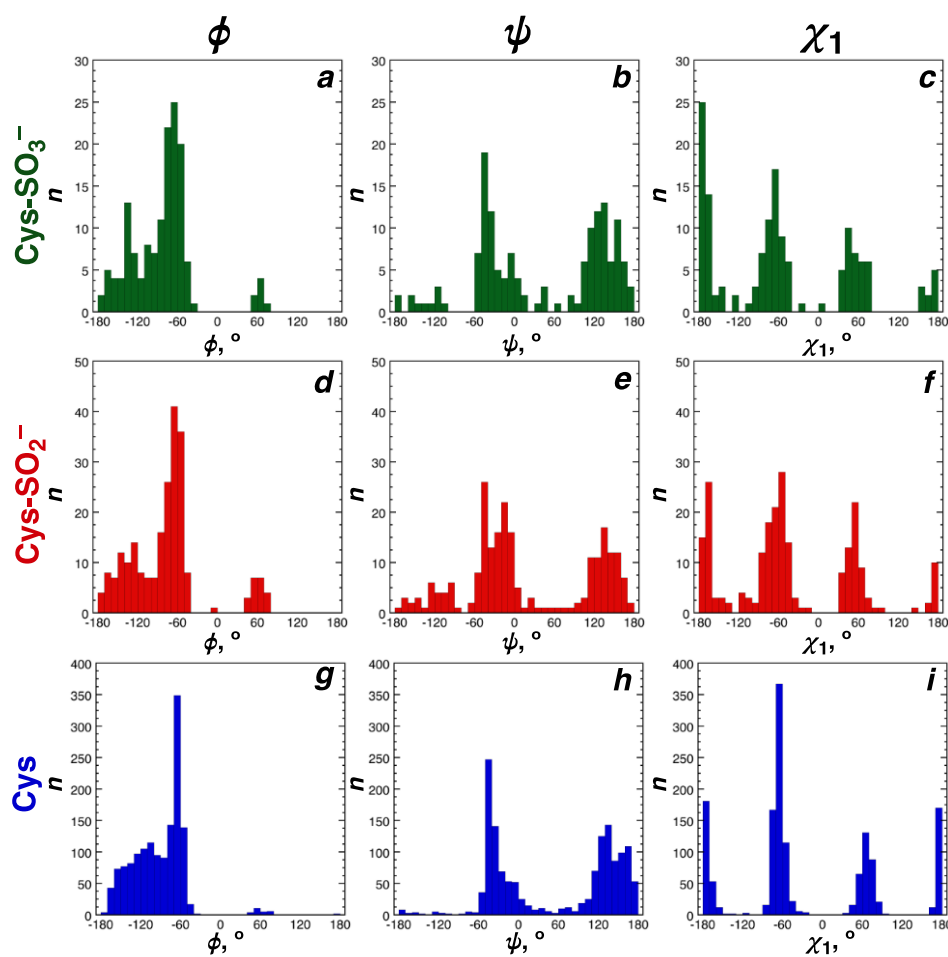
Figure 14. Histograms of the ϕ, ψ, and χ_1 dihedral angles in cysteine sulfonic acid, cysteine sulfinic acid, and cysteine residues in the PDB. The distribution of the dihedral angles ϕ, ψ, and χ_1 in three oxoforms of cysteine: (a, b, c) cysteine sulfonic acid (Cys-SO$_3^-$), (d, e, f) cysteine sulfinic acid (Cys-SO$_2^-$), and (g, h, i) cysteine (Cys-SH). The histograms represent the dihedral angles in bins of 10º.
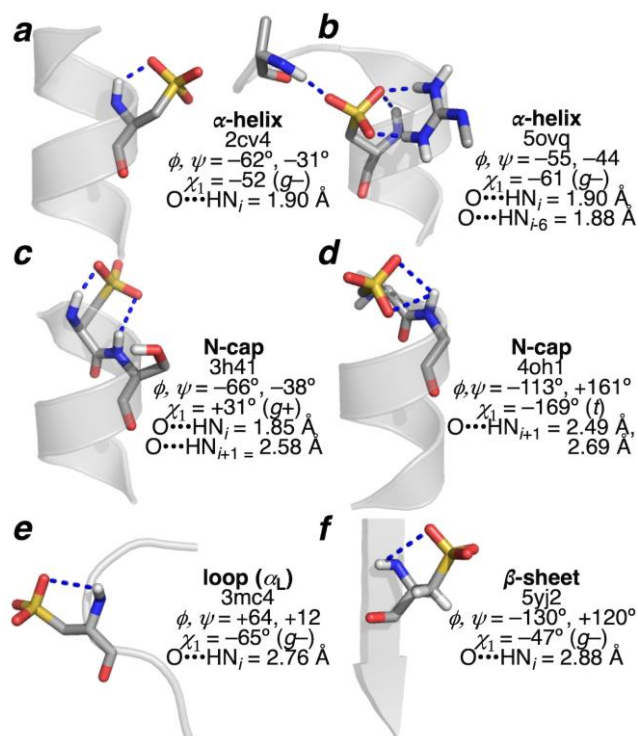
Figure 15. Representative structures of cysteine sulfonic acid in the PDB. The sulfonate side chain of cysteine sulfonic acid can be accommodated in various conformations in Ramachandran space, depending on its interactions with the protein backbone and nearby residues. (a) Cys-SO$_3^-$ (OCS50, pdb 2cv4) is located at the second residue of an α-helix and forms a hydrogen bond between one of the sulfonate oxygens and the amide NH of the same residue. (b) Cys-SO$_3^-$ (OCS49, pdb 5ovq) forms hydrogen bonds involving all three sulfonate oxygens, with the amide NH of the same residue, the amide of the residue 6 amino acids prior to Cys-SO$_3$ (i–6 residue), and the arginine side chain of a neighboring residue. (c) Cys-SO$_3^-$ (OCS238, pdb 3h41) is the first residue of an α-helix, with two hydrogen bonds that function as an α-helical N-cap and thus promote the nucleation of the α-helix. One sulfonate oxygen interacts with the amide NH of the same residue, forming an O•••H-N$_i$ hydrogen bond, and another sulfonate oxygen interacts with the amide NH of the following residue, forming an O•••H-N$_{i+1}$ hydrogen bond. (d) Cys-SO$_3^-$ (OCS45, pdb 4oh1) is near the N-terminus of an α-helix and engages in two hydrogen bonds. The amide NH of the $i+1$ residue interacts with two sulfonate oxygens, forming two O•••H-N$_{i+1}$ hydrogen bonds. (e) Cys-SO$_3^-$ (OCS219, pdb 4oh1) is in a loop and does not engage in backbone hydrogen bonds, but one of the sulfonate oxygens forms a hydrogen bond with the lysine side chain of the following residue. (f) Cys-SO$_3^-$ (OCS305, pdb 5yj2) is near the middle of a β-sheet and engages in a hydrogen bond between one of the sulfonate oxygens and the amide NH of the same residue.
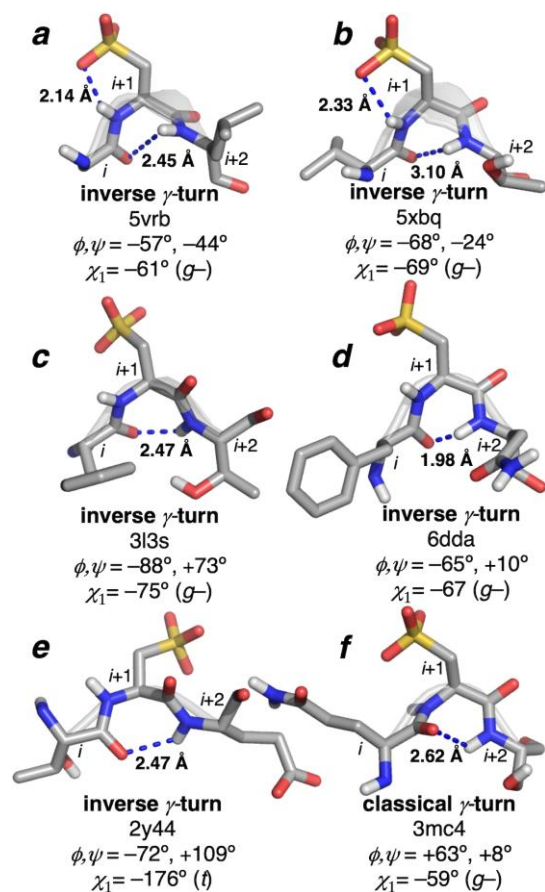
42

Figure 16. Cysteine sulfonic acid in γ-turns in the PDB. (a–e) Inverse γ-turns and (f) classical γ-turns. In these structures, cysteine sulfonate is the $i+1$ residue of a γ-turn, where the carbonyl of the i residue forms a hydrogen bond with the backbone amide hydrogen of the $i+2$ residue.
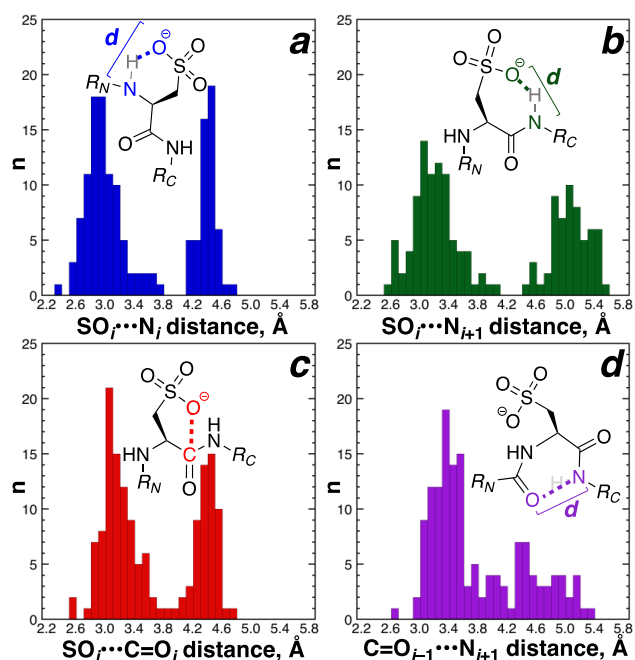
Figure 17. Side chain-main chain interaction distances of cysteine sulfonic acid in the PDB. (a) Histogram of the minimum distance between any sulfonate oxygen and the amide nitrogen of the same residue ($SO_i \cdots N_i$ distance, d). In 58% of Cys-SO_3^- residues, the $O \cdots NH_i$ distances are less than 3.3 Å, consistent with a sulfonate$\cdots$amide hydrogen bond. (b) Histogram of the minimum distance between any sulfonate oxygen and the amide nitrogen of the subsequent residue ($SO_i \cdots N_{i+1}$ distance, d). In 40% of residues, the $SO_i \cdots N_{i+1}$ distances are less than 3.3 Å. Overall, 81% of Cys-SO_3^- residues have at least one sulfonate oxygen that is in hydrogen-bonding distance with any of the NH_i and/or NH_{i+i} amides, with 41% of Cys-SO_3^- interacting only with the intraresidue (i) amide, 23% of Cys-SO_3^- interacting only with the subsequent-residue (i+1) amide, and with 16% of Cys-SO_3^- residues interacting with both the i and i+1 amides. (c) Histogram of the minimum distance between any sulfonate oxygen and the carbonyl carbon of the same residue ($SO_i \cdots C=O_i$ distance, d). In 38% of residues, the $SO_i \cdots C=O_i$ distances are ≤ 3.22 Å, the sum of the van der Waals radii of carbon and oxygen. (d) Histogram of the minimum distance between the carbonyl oxygen of the previous residue and amide nitrogen of the subsequent residue ($C=O_{i-1} \cdots N_{i+1}$ distances, d). The carbonyl oxygen of the previous residue was within 3.3 Å of the subsequent-residue amide nitrogen in 25% of structures in whic Cys-SO_3^- was the center residue, consistent with a γ-turn hydrogen bonding pattern.
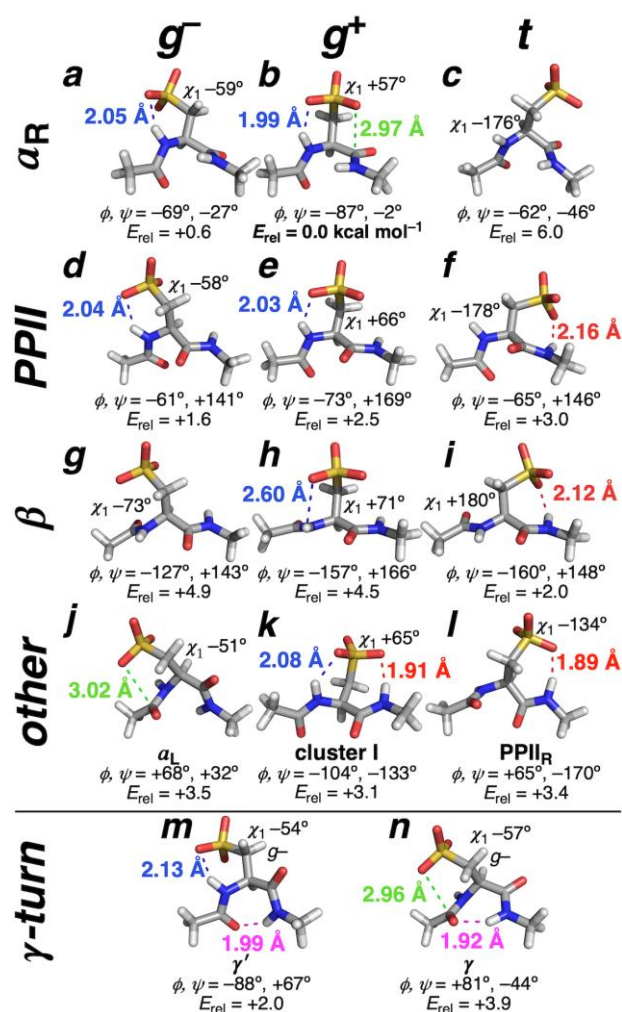
Figure 18. Computational analysis of the conformational preferences in Ac-Cys(SO₃⁻)-NHMe model as a function of region of Ramachandran space and χ_1 torsion angle. Structures and relative energies were obtained as a function of main chain and side chain conformation, via geometry optimization using DFT methods. The relative energy in kcal mol⁻¹ is indicated for each conformation, compared to the global energy minimum, defined as $E_{rel} = 0.0$ kcal mol⁻¹. The distances in Å between atoms are color-coded to indicate the type of interactions, including a hydrogen bond between a sulfonate oxygen and the amide nitrogen of the same residue (SO$_i$•••HN$_i$, blue), a hydrogen bond between a sulfonate oxygen and the amide nitrogen of the next residue (SO$_i$•••HN$_{i+1}$, red), an $n\rightarrow\pi^*$ interaction between a sulfonate oxygen and the carbonyl carbon of the same residue (SO$_i$•••CO$_i$, green), and a hydrogen bond between the carbonyl oxygen of the previous residue and the amide nitrogen of the next residue (CO$_{i-1}$•••HN$_{i+1}$, purple). Energies do not account for changes in hydrogen bonding to solvent, and thus structures with intramolecular hydrogen bonding inherently appear to have lower energies. Coordinates for these conformations are in the Supporting Information. The calculations were conducted using the M06-2X DFT functional and the 6-311++G(2d,2p) basis set in implicit H_2O (IEFPCM).

45
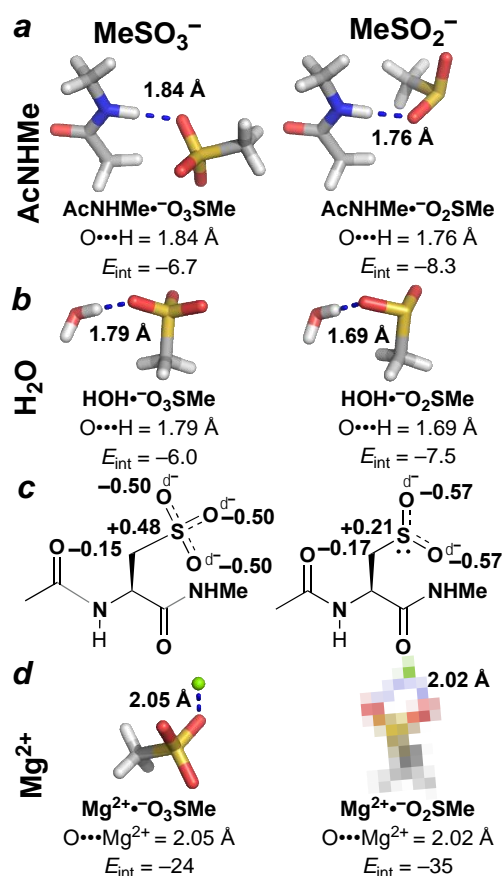
Figure 19. Computational analysis of interactions of methyl sulfonate and methyl sulfinate with an amide, water, and a magnesium ion. Calculated O•••H hydrogen bond distances and O•••Mg^{2+} distances from geometry-optimized structures are indicated. The interaction energies (E_{int}, kcal mol^{-1}) of complex formation (complex E_{int}) were calculated by subtracting the energies of each individually optimized component from the energy of the complex. (a) The geometry-optimized complexes of MeSO$_3^-$ and MeSO$_2^-$ with AcNHMe. (b) The geometry-optimized complexes of MeSO$_3^-$ and MeSO$_2^-$ with H$_2$O. (c) The calculated CM5 charges on C$^\beta$, S, and O atoms of Ac-Cys-SO$_3^-$-NHMe and Ac-Cys-SO$_2^-$-NHMe. (d) The geometry-optimized complexes of MeSO$_3^-$ and MeSO$_2^-$ with Mg^{2+}. The geometry optimization calculations were conducted using the M06-2X method with the aug-cc-pVTZ basis set in implicit H$_2$O (IEFPCM); all coordinated are in the Supporting Information. The energy calculations were conducted on these optimized structures using the MP2 method and the aug-cc-pVQZ basis set in implicit H$_2$O (IEFPCM).
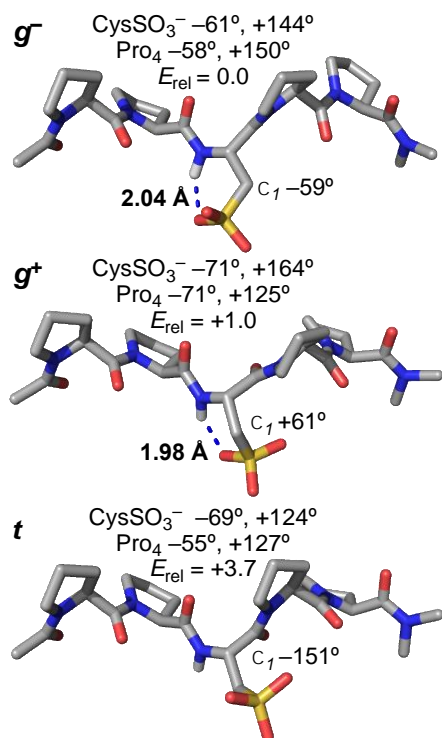
Figure 20. Computational analysis of a PPII helix model peptide (Ac-ProPro-CysSO₃⁻-ProPro-NMe₂) as a function of cysteine sulfonate χ_1 side-chain rotamer. Three minimal models of the peptide in a PPII conformation, with all proline residues with an *exo* ring pucker and *trans* amide conformation, and with the CysSO₃⁻ side-chain in g^-, g^+ and t rotamers, were generated via geometry optimization using the M06-2X method and the 6-31+G(d, p) basis set in implicit H₂O (IEFPCM). The relative energies of the peptides (E_{rel} kcal mol⁻¹) were calculated by subtracting the energy of each structure from the energy of the structure with the lowest energy (cysteine sulfonate with χ_1 g^- rotamer).
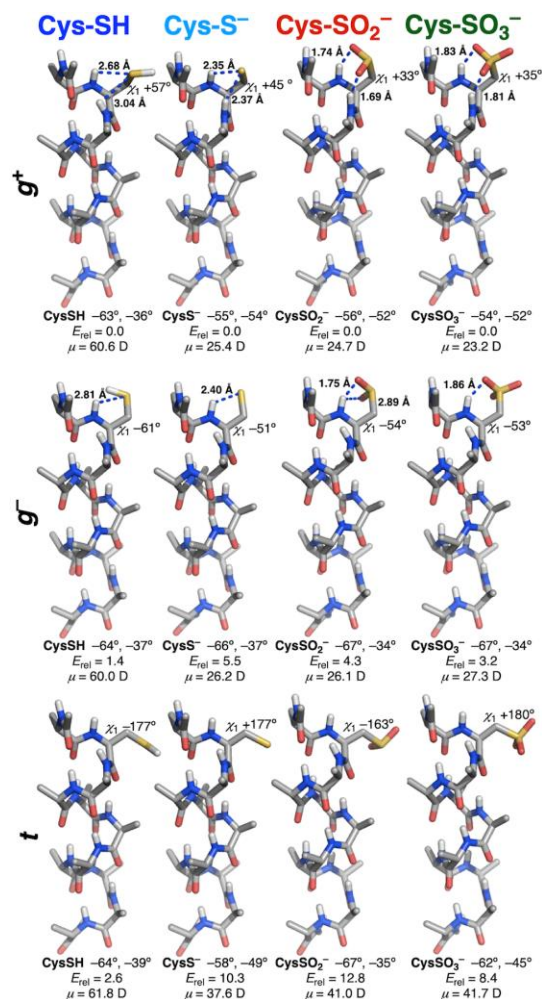
Figure 21. Computational analysis of the structures of cysteine, cysteine sulfinate, and cysteine sulfonate in an α-helical peptide model as a function of Cys χ_1 rotamer. The geometry optimization calculations were conducted on minimal α-helical models, Ac-Ala-X-Ala$_9$-NHMe, where X represents the different oxoforms of cysteine (Cys-SH, Cys-S$^-$, Cys-SO$_2^-$, and Cys-SO$_3^-$). The calculations were performed using the M11-L DFT functional and the Def2SVP basis set in implicit H$_2$O (IEFPCM). The relative energies of the peptides (E_{rel}, kcal mol^{-1}) were calculated by subtracting the energy of each structure from the energy of the structure with the lowest energy (χ_1 g^+ rotamer). The calculated dipole moment (D, Debye) for each structure is indicated. The ϕ and ψ torsion angles of the cysteine oxoforms of the respective structures are indicated. Observed SO$_i$•••HN$_i$, SO$_i$•••HN$_{i+1}$, S$_i$•••HN$_i$, and S$_i$•••HN$_{i+1}$ hydrogen bond distances (Å) are indicated.

Tables

Ac-GPP**X**PPGY-NH$_2$ X=	$[\theta]_{228}$, deg cm^2 dmol^{-1}	λ_{max}, nm	$[\theta]$ at λ_{max}, deg cm^2 dmol^{-1}
Pro	3000	230	3070
Cys-SH	−680	232	−240
Cys-S$^-$	−530	233	−260
Cys-SO$_2^-$	340	231	1290
Cys-SO$_3^-$	310	230	340

Table 1. Summary of circular dichroism data for the polyproline II helix propagation model peptide Ac-GPPXPPGY-NH$_2$. CD data for peptides with X= Cys-SO$_3^-$ were recorded on solutions at pH 7 in 5 mM phosphate buffer with 25 mM KF at 25 ºC. For other peptides, data were collected at pH 4 in 5 mM phosphate buffer with 25 mM KF at 25 ºC. Polyproline II helix (PPII) population is indicated by the magnitude of the local maximum magnitude near 228 nm. The data with standard errors are in Table S6.

Ac-GPP**X**PPGY-NH$_2$ X=	$^3J_{\alpha N}$, Hz	δ, H^N, ppm	δ, H$^\alpha$, ppm	δ, H$^\beta$, ppm
Cys-SH	7.2	8.40	4.73	2.85, 2.80
Cys-SO$_2^-$	6.3	8.59	4.78	2.72, 2.45
Cys-SO$_3^-$	6.0	8.31	4.88	3.18

Table 2. Summary of ^{1}H NMR data in Ac-GPPXPPGY-NH$_2$ peptides with X = Cys-SH, Cys-SO$_2^-$, and Cys-SO$_3^-$. ^{1}H NMR data were recorded on solutions at pH 4 in 5 mM phosphate buffer with 25 mM NaCl and 10% D$_2$O at 300 K. $^3J_{\alpha N}$ is the vicinal coupling constant between the amide (H^N) and alpha (H$^\alpha$) hydrogens of the same residue. $^3J_{\alpha N}$ was not determined for Cys-S$^-$ due to rapid amide proton exchange at pH 8.

Ac-**X**PPGY-NH$_2$ X=	$[\theta]_{228}$, deg cm^2 dmol^{-1}	λ_{max}, nm	$[\theta]$ at λ_{max}, deg cm^2 dmol^{-1}
Ala	3180	227	3260
Cys-SH	1120	230	1190
Cys-S$^-$	2400	226	2540
Cys-SO$_2^-$	2690	232	2980
Cys-SO$_3^-$	2340	227	2380

Table 3. Summary of circular dichroism data for the polyproline II helix initiation model peptide Ac-XPPGY-NH$_2$. CD data were recorded on solutions at pH 7 in 5 mM phosphate buffer with 25 mM KF at 25 ºC. The data with standard errors are shown in Table S7.

Ac-**X**PPGY-NH$_2$ X=	X, $^3J_{\alpha N}$, Hz	δ, H^N, ppm	δ, H$^\alpha$, ppm	δ, H$^\beta$, ppm
Ala	6.0	8.18	4.52	1.28
Cys-SH	7.1	8.31	4.76	2.90, 2.82
Cys-SO$_2^-$	6.6	8.51	4.83	2.73, 2.45
Cys-SO$_3^-$	6.7	8.37	4.96	3.19

Table 4. Summary of ^{1}H NMR data in Ac-XPPGY-NH$_2$ peptides with X = Cys-SH, Cys-SO$_2^-$, and Cys-SO$_3^-$. ^{1}H NMR data were recorded on solutions at pH 4 in 5 mM phosphate buffer with 25 mM NaCl and 10% D$_2$O at 300 K. $^3J_{\alpha N}$ was not determined for Cys-S$^-$ due to rapid amide proton exchange at pH 8.

Ac-A**X**AAA AKAAAAK AAGY-NH$_2$ X=	$[\theta]_{208}$, deg cm^2 dmol^{-1}	$[\theta]_{222}$, deg cm^2 dmol^{-1}	$[\theta]_{190}$, deg cm^2 dmol^{-1}	$[\theta]_{222}/$ $[\theta]_{208}$	$-[\theta]_{190}/$ $[\theta]_{208}$	% α-helicity
Lys	−18800	−17800	31500	0.95	1.68	53
Cys-SH	−18600	−17300	28400	0.93	1.53	51
Cys-S$^-$	−20600	−20200	38000	0.97	1.85	60
Cys-SO$_2^-$	−24100	−24200	51600	1.00	2.01	72
Cys-SO$_3^-$	−21200	−20800	38900	0.98	1.83	62

Table 5. Summary of circular dichroism data for peptides with cysteine oxoforms in a model peptide of an α-helix. CD data for the peptides Ac-A**X**AAAAKAAAAKAAGY-NH$_2$, X = Cys-SO$_3^-$ pH 7, Cys-SH pH 4, and Cys-S$^-$ pH 8.5 were collected in 5 mM phosphate buffer with 25 mM KF at 20 ºC and 0.5 ºC. The percent α-helicity was calculated as (100% × $[\theta]_{222}$)/(−40000 × (1–2.5/16)).[62] The data with standard errors are in Table S8.

Ac-A**X**AAA AKAAAAK AAGY-NH$_2$ X=	**X,** $^3J_{\alpha N}$, **Hz**	δ, H^N, ppm	δ, H$^\alpha$, ppm	δ, H$^\beta$, ppm
Cys-SH	5.4	8.71	4.41	2.98
Cys-SO$_2^-$	-^{a}	8.86	4.60	2.89, 2.66
Cys-SO$_3^-$	6.7	8.58	4.79	3.42

Table 6. Summary of ^{1}H NMR data in Ac-AXAAAAKAAAAKAAGY-NH$_2$ peptides with X = Cys-SH, Cys-SO$_2^-$, and Cys-SO$_3^-$. NMR data were collected at pH 4 in 5 mM phosphate buffer with 25 mM NaCl at 274 K. ^{a} H^N peaks were broadened for cysteine sulfinate, precluding the measurement of the $^3J_{\alpha N}$.

residue	α_R	β	PPII	PPII$_R$	α_L	other	total residues/ structures
Cys-SO$_3^-$	59 40.4%	48 32.9%	28 19.2%	5 3.4%	2 1.4%	4 2.7%	146/141
Cys-SO$_2^-$	108 47.8%	66 29.2%	22 9.7%	15 6.6%	6 2.7%	9 4.0%	226/216
Cys	605 41.4%	564 38.6%	196 13.4%	6 0.4%	20 1.4%	69 4.7%	1460/431

Table 7. Summary of the observed conformations of cysteine sulfonic acid, cysteine sulfinic acid, and cysteine residues in the PDB. The regions of the Ramachandran plot for this analysis are defined as follows: α-helical (α_R): ($-110° \leq \phi \leq -30°$, $-80° \leq \psi \leq +30°$); β/extended: ($-180°$ $< \phi < -90°$ and [$\psi \leq -120°$ or $+180° > \psi \geq +60°$]); PPII: ($-90° \leq \phi \leq -40°$ and $+100° \leq \psi \leq +180°$); PPII$_R$: ($+30° \leq \phi \leq +90°$ and $-180° \leq \psi \leq -90°$); and α_L: ($+30° \leq \phi \leq +110°$ and $-30° \leq \psi \leq +80°$).

	g– %	t %	g+ %
Cys-SO$_3^-$	38	38	24
Cys-SO$_2^-$	47	27	25
Cys	48	30	22

Table 8. Distribution of χ_1 of cysteine oxoforms in the PDB. Side-chain rotamers are defined based on the χ_1 dihedral angle, with the g^- rotamer defined as ($-120° \leq \chi_1° < 0°$), the t rotamer defined as ($+120° \leq \chi_1° < -120°$), and the g^+ rotamer defined as ($0° \leq \chi_1° < +120°$).

References

(1)   Reddie, K. G.; Carroll, K. S. Expanding the functional diversity of proteins through cysteine oxidation. *Curr. Opin. Chem. Biol.* **2008**, *12*, 746-754.

(2)   Paulsen, C. E.; Carroll, K. S. Cysteine-Mediated Redox Signaling: Chemistry, Biology, and Tools for Discovery. *Chem. Rev.* **2013**, *113*, 4633-4679.

(3)   Go, Y. M.; Chandler, J. D.; Jones, D. P. The cysteine proteome. *Free Radic. Biol. Med.* **2015**, *84*, 227-245.

(4)   Poole, L. B. The basics of thiols and cysteines in redox biology and chemistry. *Free Radic. Biol. Med.* **2015**, *80*, 148-157.

(5)   Alcock, L. J.; Perkins, M. V.; Chalker, J. M. Chemical methods for mapping cysteine oxidation. *Chem. Soc. Rev.* **2018**, *47*, 231-268.

(6)   Bartberger, M. D.; Mannion, J. D.; Powell, S. C.; Stamler, J. S.; Houk, K. N.; Toone, E. J. S-N Dissociation Energies of S-Nitrosothiols: On the Origins of Nitrosothiol Decomposition Rates. *J. Am. Chem. Soc.* **2001**, *123*, 8868-8869.

(7)   Lei, K.; Townsend, D. M.; Tew, K. D. Protein cysteine sulfinic acid reductase (sulfiredoxin) as a regulator of cell proliferation and drug response. *Oncogene* **2008**, *27*, 4877-4887.

(8)   Lowther, W. T.; Haynes, A. C. Reduction of Cysteine Sulfinic Acid in Eukaryotic, Typical 2-Cys Peroxiredoxins by Sulfiredoxin. *Antioxid. Redox Signaling* **2011**, *15*, 99-109.

(9)   Akter, S.; Fu, L.; Jung, Y.; Lo Conte, M.; Lawson, J. R.; Lowther, W. T.; Sun, R.; Liu, K. K.; Yang, J.; Carroll, K. S. Chemical proteomics reveals new targets of cysteine sulfinic acid reductase. *Nat. Chem. Biol.* **2018**, *14*, 995-1004.

(10)   Kehm, R.; Baldensperger, T.; Raupbach, J.; Hohn, A. Protein oxidation-Formation mechanisms, detection and relevance as biomarkers in human diseases. *Redox Biol.* **2021**, *42*, 101901.

(11)   Rookyard, A. W.; Paulech, J.; Thyssen, S.; Liddy, K. A.; Puckeridge, M.; Li, D. K.; White, M. Y.; Cordwell, S. J. A Global Profile of Reversible and Irreversible Cysteine Redox Post-Translational Modifications During Myocardial Ischemia/Reperfusion Injury and Antioxidant Intervention. *Antioxid. Redox Signaling* **2021**, *34*, 11-31.

(12)   Fujiwara, N.; Nakano, M.; Kato, S.; Yoshihara, D.; Ookawara, T.; Eguchi, H.; Taniguchi, N.; Suzuki, K. Oxidative modification to cysteine sulfonic acid of Cys(111) in human copper-zinc superoxide dismutase. *J. Biol. Chem.* **2007**, *282*, 35933-35944.

(13)   Fujiwara, N.; Yoshihara, D.; Sakiyama, H.; Eguchi, H.; Suzuki, K. Solution oxygen-17 NMR application for observing a peroxidized cysteine residue in oxidized human SOD1. *Hyperfine Interact.* **2016**, *237*, 114.

(14)   Bakavayev, S.; Argueti, S.; Venkatachalam, N.; Yehezkel, G.; Stavsky, A.; Barak, Z.; Israelson, A.; Engel, S. Exposure of beta 6/beta 7-Loop in Zn/Cu Superoxide Dismutase (SOD1) Is Coupled to Metal Loss and Is Transiently Reversible During Misfolding. *ACS Chem. Neurosci.* **2021**, *12*, 49-62.

(15)   Baek, Y.; Woo, T. G.; Ahn, J.; Lee, D.; Kwon, Y.; Park, B. J.; Ha, N. C. Structural analysis of the overoxidized Cu/Zn-superoxide dismutase in ROS-induced ALS filament formation. *Commun. Biol.* **2022**, *5*.

(16)   Ishida, Y.; Aki, M.; Fujiwara, S.; Nagahama, M.; Ogasawara, Y. Peroxidatic cysteine residue of peroxiredoxin 2 separated from human red blood cells treated by tert-butyl hydroperoxide is hyperoxidized into sulfinic and sulfonic acids. *Human Cell* **2017**, *30*, 279-289.

(17)   Tomin, T.; Schittmayer, M.; Honeder, S.; Heininger, C.; Birner-Gruenberger, R. Irreversible oxidative post-translational modifications in heart disease. *Expert Rev. Proteomics* **2019**, *16*, 681-693.

(18)   Paramasivan, S.; Adav, S. S.; Ngan, S. C.; Dalan, R.; Leow, M. K. S.; Ho, H. H.; Sze, S. K. Serum albumin cysteine trioxidation is a potential oxidative stress biomarker of type 2 diabetes mellitus. *Sci. Rep.* **2020**, *10*, 6475.

(19)   Saletti, R.; Reina, S.; Pittala, M. G. G.; Magri, A.; Cunsolo, V.; Foti, S.; De Pinto, V. Post-translational modifications of VDAC1 and VDAC2 cysteines from rat liver mitochondria. *Biochim. Biophys. Acta Bioenerg.* **2018**, *1859*, 806-816.

(20)   Reina, S.; Pittala, M. G. G.; Guarino, F.; Messina, A.; De Pinto, V.; Foti, S.; Saletti, R. Cysteine Oxidations in Mitochondrial Membrane Proteins: The Case of VDAC Isoforms in Mammals. *Front. Cell. Dev. Biol.* **2020**, *8*, 397.

(21)   Seo, J. H.; Lim, J. C.; Lee, D. Y.; Kim, K. S.; Piszczek, G.; Nam, H. W.; Kim, Y. S.; Ahn, T.; Yun, C. H.; Kim, K.; Chock, P. B.; Chae, H. Z. Novel Protective Mechanism against Irreversible Hyperoxidation of Peroxiredoxin N-alpha-TERMINAL ACETYLATION OF HUMAN PEROXIREDOXIN II. *J. Biol. Chem.* **2009**, *284*, 13455-13465.

(22)   Liu, W. X.; Liu, A. J.; Gao, H. L.; Wang, Q.; Wang, L. M.; Warkentin, E.; Rao, Z. H.; Michel, H.; Peng, G. H. Structural properties of the peroxiredoxin AhpC2 from the hyperthermophilic eubacterium Aquifex aeolicus. *Biochim. Biophys. Acta Gen. Subj.* **2018**, *1862*, 2797-2805.

(23)   Lian, F. M.; Jiang, Y. L.; Yang, W. C.; Yang, X. W. Crystal structure of sulfonic peroxiredoxin Ahp1 in complex with thioredoxin Trx2 mimics a conformational intermediate during the catalytic cycle. *Int. J. Biol. Macromol.* **2020**, *161*, 1055-1060.

(24)   Elko, E. A.; Manuel, A. M.; White, S.; Zito, E.; van Der Vliet, A.; Anathy, V.; Janssen-Heininger, Y. M. W. Oxidation of peroxiredoxin-4 induces oligomerization and promotes interaction with proteins governing protein folding and endoplasmic reticulum stress. *J. Biol. Chem.* **2021**, *296*, 100665.

(25)   Chen, C. H.; Li, W. Z.; Sultana, R.; You, M. H.; Kondo, A.; Shahpasand, K.; Kim, B. M.; Luo, M. L.; Nechama, M.; Lin, Y. M.; Yao, Y. D.; Lee, T. H.; Zhou, X. Z.; Swomley, A. M.; Butterfield, D. A.; Zhang, Y.; Lu, K. P. Pin1 cysteine-113 oxidation inhibits its catalytic activity and cellular function in Alzheimer's disease. *Neurobiol. Dis.* **2015**, *76*, 13-23.

(26)   Men, L.; Wang, Y. S. The oxidation of yeast alcohol dehydrogenase-1 by hydrogen peroxide in vitro. *J. Proteome Res.* **2007**, *6*, 216-225.

(27)   Hamann, M.; Zhang, T. Q.; Hendrich, S.; Thomas, J. A. Quantitation of protein sulfinic and sulfonic acid, irreversibly oxidized protein cysteine sites in cellular proteins. *Meth. Enzymol.* **2002**, *348*, 146-156.

(28)   Chang, Y. C.; Huang, C. N.; Lin, C. H.; Chang, H. C.; Wu, C. C. Mapping protein cysteine sulfonic acid modifications with specific enrichment and mass spectrometry: An integrated approach to explore the cysteine oxidation. *Proteomics* **2010**, *10*, 2961-2971.

(29)   Mueller, M.; Kratzer, R.; Schiller, M.; Slavica, A.; Rechberger, G.; Kollroser, M.; Nidetzky, B. The role of Cys108 in Trigonopsis variabilis D-amino acid oxidase examined through chemical oxidation studies and point mutations C108S and C108D. *Biochim. Biophys. Acta Proteins Proteom.* **2010**, *1804*, 1483-1491.

(30)   Schmidt, F.; Dahlmann, B.; Hustoft, H. K.; Koehler, C. J.; Strozynski, M.; Kloss, A.; Zimny-Arndt, U.; Jungblut, P. R.; Thiede, B. Quantitative proteome analysis of the 20S proteasome of apoptotic Jurkat T cells. *Amino Acids* **2011**, *41*, 351-361.

(31)   Lee, C. F.; Paull, T. T.; Person, M. D. Proteome-wide Detection and Quantitative Analysis of Irreversible Cysteine Oxidation Using Long Column UPLC-pSRM. *J. Proteome Res.* **2013**, *12*, 4302-4315.

(32)   Brewer, T. F.; Garcia, F. J.; Onak, C. S.; Carroll, K. S.; Chang, C. J. Chemical Approaches to Discovery and Study of Sources and Targets of Hydrogen Peroxide Redox Signaling Through NADVII Oxidase Proteins. *Ann. Rev. Biochem.* **2015**, *84*, 765-790.

(33)   Lennicke, C.; Rahn, J.; Heimer, N.; Lichtenfels, R.; Wessjohann, L. A.; Seliger, B. Redox proteomics: Methods for the identification and enrichment of redox-modified proteins and their applications. *Proteomics* **2016**, *16*, 197-213.

(34)   Borotto, N. B.; McClory, P. J.; Martin, B. R.; Hakansson, K. Targeted Annotation of S-Sulfonylated Peptides by Selective Infrared Multiphoton Dissociation Mass Spectrometry. *Anal. Chem.* **2017**, *89*, 8304-8310.

(35)   van der Reest, J.; Lilla, S.; Zheng, L.; Zanivan, S.; Gottlieb, E. Proteome-wide analysis of cysteine oxidation reveals metabolic sensitivity to redox stress. *Nature Commun.* **2018**, *9*, 1581.

(36)   Urmey, A. R.; Zondlo, N. J. Structural Preferences of Cysteine Sulfinic Acid: the Sulfinate Engages in Multiple Local Interactions with the Peptide Backbone. *Free Radic. Biol. Med.* **2020**, *148*, 96-107.

(37)   Ruiz, D. G.; Sandoval-Perez, A.; Rangarajan, A. V.; Gunderson, E. L.; Jacobson, M. P. Cysteine Oxidation in Proteins: Structure, Biophysics, and Simulation. *Biochemistry* **2022**, *61*, 2165-2176.

(38)   Forbes, C. R.; Sinha, S. K.; Ganguly, H. K.; Bai, S.; Yap, G. P. A.; Patel, S.; Zondlo, N. J. Insights into Thiol-Aromatic Interactions: A Stereoelectronic Basis for S–H/π Interactions. *J. Am. Chem. Soc.* **2017**, *139*, 1842-1855.

(39)   Yang, C. Y.; Yang, C. F.; Tang, X. F.; Machado, L.; Singh, J. P.; Peti, W.; Chen, C. S.; Meng, T. C. Active-site cysteine 215 sulfonation targets protein tyrosine phosphatase PTP1B for Cullin1 E3 ligase-mediated degradation. *Free Radic. Biol. Med.* **2023**, *194*, 147-159.

(40)   Sanger, F. Fractionization of Oxidized Insulin. *Biochem. J.* **1949**, *44*, 126-128.

(41)   Hirs, C. H. W. Performic acid oxidation. *Meth. Enzymol.* **1967**, *11*, 197-199.

(42)   Williams, B. J.; Barlow, C. K.; Kmiec, K. L.; Russell, W. K.; Russell, D. H. Negative Ion Fragmentation of Cysteic Acid Containing Peptides: Cysteic Acid as a Fixed Negative Charge. *J. Am. Soc. Mass. Spec.* **2011**, *22*, 1622-1630.

(43)   Lu, D. D.; Jin, Y. Y.; Wang, X. Y.; Xie, L. Y.; Liu, Q. Q.; Chen, Y. M.; Wang, H.; Lei, Z. Q. Heparin-like anticoagulant polypeptides with tunable activity: Synthesis, characterization, anticoagulative properties and clot solubilities in vitro. *Mater. Sci. Eng. C Mater. Biol. Appl.* **2021**, *129*, 112405.

(44)   Urmey, A. R.; Zondlo, N. J. Synthesis of Peptides with Cysteine Sulfinic Acid via the Cysteine Methoxybenzyl Sulfone. *Peptide Sci.* **2020**, *112*, e24137.

(45)   Urmey, A. R.; Zondlo, N. J. Cysteine Oxidation to the Sulfinic Acid Induces Oxoform-Specific Lanthanide Binding and Fluorescence in a Designed Peptide. *Free Radic. Biol. Med.* **2020**, *152*, 166-174.

(46)   Men, L. J.; Wang, Y. S. Fragmentation of the deprotonated ions of peptides containing cysteine, cysteine sulfinic acid, cysteine sulfonic acid, aspartic acid, and glutamic acid. *Rapid Commun. Mass. Spec.* **2006**, *20*, 777-784.

(47)   Rostami, A.; Moradi, S.; Shokri, Z. Fe3O4 as a magnetically reusable Fenton nanocatalyst for the oxidation of thiols to sulfonic acid and sulfides to sulfoxides and sulfones. *Comptes Rendus Chimie* **2018**, *21*, 80-87.

(48)   Parida, K. N.; Chandra, A.; Moorthy, J. N. Oxidation of thiols to sulphonic acids with Oxone((R))/NaHCO3 and KBrO3. *ChemistrySelect* **2016**, *1*, 490-494.

(49)   Romão, C. C.; Kühn, F. E.; Herrmann, W. A. Rhenium(VII) Oxo and Imido Complexes: Synthesis, Structures, and Applications. *Chem. Rev.* **1997**, *97*, 3197-3246.

(50)   Wang, Y.; Espenson, J. H. Oxidation of symmetric disulfides with hydrogen peroxide catalyzed by methyltrioxorhenium(VII). *J. Org. Chem.* **2000**, *65*, 104-107.

(51)   Ballistreri, F. P.; Tomaselli, G. A.; Toscano, R. M. Selective and mild oxidation of thiols to sulfonic acids by hydrogen peroxide catalyzed by methyltrioxorhenium. *Tetrahedron Lett.* **2008**, *49*, 3291-3293.

(52)   Ballistreri, F. P.; Tomaselli, G. A.; Toscano, R. M. Selective oxidation reactions of diaryl- and dialkyldisulfides to sulfonic acids by CH3ReO3/hydrogen peroxide. *Tetrahedron Lett.* **2009**, *50*, 6231-6232.

(53)   Forbes, C. R.; Zondlo, N. J. Synthesis of Thiophenylalanine-Containing Peptides via Cu(I)-mediated Cross-Coupling. *Org. Lett.* **2012**, *14*, 464-467.

(54)   Murphy, A. B.; Duong, C. N.; Crenshaw, K. K.; Hartman, S. K.; Barrett, W. F.; Whitehead, A. R.; Lampkins, A. J.; Gregory, B. W. Catalytic oxidation of alkanethiols and dialkyldisulfides to alkanesulfonic acids by H2O2/ CH3ReO3 examined by electrospray ionization mass spectrometry. *J. Mass Spectrom.* **2014**, *49*, 241-247.

(55)   Lazzaro, F.; Crucianelli, M.; De Angelis, F.; Neri, V.; Saladino, R. A novel oxidative side-chain transformation of a-amino acids and peptides by methyltrioxorhenium/H2O2 system. *Tetrahedron Lett.* **2004**, *45*, 9237-9240.

(56)   Brown, A. M.; Zondlo, N. J. A Propensity Scale for Type II Polyproline Helices (PPII): Aromatic Amino Acids in Proline-Rich Sequences Strongly Disfavor PPII Due to Proline-Aromatic Interactions. *Biochemistry* **2012**, *51*, 5041-5051.

(57)   Brister, M. A.; Pandey, A. K.; Bielska, A. A.; Zondlo, N. J. OGlcNAcylation and Phosphorylation Have Opposing Structural Effects in tau: Phosphothreonine Induces Particular Conformational Order. *J. Am. Chem. Soc.* **2014**, *136*, 3803-3816.

(58)   Pandey, A. K.; Thomas, K. M.; Forbes, C. R.; Zondlo, N. J. Tunable Control of Polyproline Helix (PPII) Structure via Aromatic Electronic Effects: An Electronic Switch of Polyproline Helix. *Biochemistry* **2014**, *53*, 5307-5314.

(59)   Tressler, C. M.; Zondlo, N. J. (2S,4R)- and (2S,4S)-Perfluoro-tert-butyl 4-Hydroxyproline: Two Conformationally Distinct Proline Amino Acids for Sensitive Application in 19F NMR. *J. Org. Chem.* **2014**, *79*, 5880-5886.

(60)   Tressler, C. M.; Zondlo, N. J. Perfluoro-tert-butyl Homoserine is a Helix-Promoting, Highly Fluorinated, NMR-Sensitive Aliphatic Amino Acid: Detection of the Estrogen Receptor•Coactivator Protein-Protein Interaction by 19F NMR. *Biochemistry* **2017**, *56*, 1062-1074.

(61)   Marqusee, S.; Robbins, V. H.; Baldwin, R. L. Unusually stable helix formation in short alanine-based peptides. *Proc. Natl. Acad. Sci. USA* **1989**, *86*, 5286-5290.

(62)   Cochran, D. A. E.; Doig, A. J. Effect of the N2 residue on the stability of the alpha-helix for all 20 amino acids. *Protein Sci.* **2001**, *10*, 1305-1311.

(63)   Elbaum, M. B.; Zondlo, N. J. OGlcNAcylation and Phosphorylation Have Similar Structural Effects in α-Helices: Post-Translational Modifications as Inducible Start and Stop Signals in α-Helices, with Greater Structural Effects on Threonine Modification. *Biochemistry* **2014**, *53*, 2242-2260.

(64)   Iqbalsyah, T. M.; Doig, A. J. Effect of the N3 residue on the stability of the alpha-helix. *Protein Science* **2004**, *13*, 32-39.

(65)   Thomas, K. M.; Naduthambi, D.; Tririya, G.; Zondlo, N. J. Proline Editing: A Divergent Strategy for the Synthesis of Conformationally Diverse Peptides. *Org. Lett.* **2005**, *7*, 2397-2400.

(66)   Pandey, A. K.; Naduthambi, D.; Thomas, K. M.; Zondlo, N. J. Proline Editing: A General and Practical Approach to the Synthesis of Functionally and Structurally Diverse Peptides. Analysis of Steric versus Stereoelectronic Effects of 4-Substituted Prolines on Conformation within Peptides. *J. Am. Chem. Soc.* **2013**, *135*, 4333-4363.

(67)   Isidro-Llobet, A.; Alvarez, M.; Albericio, F. Amino Acid-Protecting Groups. *Chem. Rev.* **2009**, *109*, 2455-2504.

(68)   Woody, R. W. Circular Dichroism Spectrum of Peptides in the Poly(Pro)II Conformation. *J. Am. Chem. Soc.* **2009**, *131*, 8234-8245.

(69)   Rucker, A. L.; Pager, C. T.; Campbell, M. N.; Qualls, J. E.; Creamer, T. P. Host-Guest Scale of Left-Handed Polyproline II Helix Formation. *Proteins* **2003**, *53*, 68-75.

(70)   Shi, Z. S.; Olson, C. A.; Rose, G. D.; Baldwin, R. L.; Kallenbach, N. R. Polyproline II structure in a sequence of seven alanine residues. *Proc. Natl. Acad. Sci. USA* **2002**, *99*, 9190-9195.

(71)   Ding, L.; Chen, K.; Santini, P. A.; Shi, Z.; Kallenbach, N. R. The Pentapeptide GGAGG Has PII Conformation. *J. Am. Chem. Soc.* **2003**, *125*, 8092-8093.

(72)   Shi, Z.; Chen, K.; Liu, Z.; Ng, A.; Bracken, W. C.; Kallenbach, N. R. Polyproline II propensities from GGXGG peptides reveal an anticorrelation with b-sheet scales. *Proc. Natl. Acad. Sci. USA* **2005**, *102*, 17964-17968.

(73)   Pandey, A. K.; Ganguly, H. K.; Sinha, S. K.; Daniels, K. E.; Yap, G. P. A.; Patel, S.; Zondlo, N. J. An Inherent Structural Difference Between Serine and Threonine Phosphorylation: Phosphothreonine Prefers an Ordered, Compact, Cyclic Conformation. *bioRxiv* **2020**, DOI: 10.1101/2020.1102.1129.971382.

(74)   Bartlett, G. J.; Choudhary, A.; Raines, R. T.; Woolfson, D. N. n->pi* interactions in proteins. *Nat. Chem. Biol.* **2010**, *6*, 615-620.

(75)   Newberry, R. W.; Raines, R. T. The n->pi* interaction. *Acc. Chem. Res.* **2017**, *50*, 1838-1846.

(76)   Wenzell, N. A.; Ganguly, H. K.; Pandey, A. K.; Bhatt, M. R.; Yap, G. P. A.; Zondlo, N. J. Electronic and steric control of n→π* interactions via N-capping: stabilization of the α-helix conformation without a hydrogen bond. *ChemBioChem* **2019**, *20*, 963-967.

(77)   Zondlo, N. J. Fold Globally, Bond Locally. *Nat. Chem. Biol.* **2010**, *6*, 567-568.

(78)   Andrew, C. D.; Warwicker, J.; Jones, G. R.; Doig, A. J. Effect of phosphorylation on a-helix stability as a function of position. *Biochemistry* **2002**, *41*, 1897-1905.

(79)   Signarvic, R. S.; DeGrado, W. F. De Novo Design of a Molecular Switch: Phosphorylation-Dependent Association of Designed Peptides. *J. Mol. Biol.* **2003**, *334*, 1-12.

(80)   Szilak, L.; Moitra, J.; Vinson, C. Design of a leucine zipper coiled coil stabilized 1.4 kcal mol^{-1} by phosphorylation of a serine in the e position. *Protein Sci.* **1997**, *6*, 1273-1283.

(81)   Aurora, R.; Rose, G. D. Helix capping. *Protein Sci.* **1998**, *7*, 21-38.

(82)   Vuister, G. W.; Bax, A. Quantitative J Correlation: A New Approach for Measuring Homonuclear Three-Bond J_{HNHa} Coupling Constants in ^{15}N-enriched Proteins. *J. Am. Chem. Soc.* **1993**, *115*, 7772-7777.

(83)   van Montfort, R. L. M.; Congreve, M.; Tisi, D.; Carr, R.; Jhoti, H. Oxidation state of the active-site cysteine in protein tyrosine phosphatase 1B. *Nature* **2003**, *423*, 773-777.

(84)   Lim, J. C.; Choi, H. I.; Park, Y. S.; Nam, H. W.; Woo, H. A.; Kwon, K. S.; Kim, Y. S.; Rhee, S. G.; Kim, K.; Chae, H. Z. Irreversible Oxidation of the Active-site Cysteine of Peroxiredoxin to Cysteine Sulfonic Acid for Enhanced Molecular Chaperone Activity. *J. Biol. Chem.* **2008**, *283*, 28873-28880.

(85)   Dunbrack, R. L., Jr.; Karplus, M. Backbone-dependent Rotamer Library for Proteins: Application to Side-chain prediction. *J. Mol. Biol.* **1993**, *230*, 543-574.

(86)   Lovell, S. C.; Word, J. M.; Richardson, J. S.; Richardson, D. C. The Penultimate Rotamer Library. *Proteins* **2000**, *40*, 389-408.

(87)   Penel, S.; Doig, A. J. Rotamer strain energy in protein helices quantification of a major force opposing protein folding. *J. Mol. Biol.* **2001**, *305*, 961-968.

(88)   Dhanasingh, I.; Sung, J. Y.; La, J. W.; Kang, E.; Lee, D. W.; Lee, S. H. Structure of oxidized pyrrolidone carboxypeptidase from Fervidobacterium islandicum AW-1 reveals unique structural features for thermostability and keratinolysis. *Biochem. Biophys. Res. Comm.* **2021**, *540*, 101-107.

(89)   Zhao, Y.; Truhlar, D. G. The M06 suite of density functionals for main group thermochemistry, thermochemical kinetics, noncovalent interactions, excited states, and transition elements: two new functionals and systematic testing of four M06-class functionals and 12 other functionals. *Theor. Chem. Acc.* **2008**, *120*, 215-241.

(90)   Raghavachari, K.; Binkley, J. S.; Seeger, R.; Pople, J. A. Self-Consistent Molecular Orbital Methods. 20. Basis sets for correlated wave functions. *J. Chem. Phys.* **1980**, *72*, 650-654.

(91)   Frisch, M. J.; Head-Gordon, M.; Pople, J. A. Direct MP2 gradient method. *Chem. Phys. Lett.* **1990**, *166*, 275-280.

(92)   Gunasekaran, K.; Ramakrishnan, C.; Balaram, P. Disallowed Ramachandran Conformations of Amino Acid Residues in Protein Structures. *J. Mol. Biol.* **1996**, *264*, 191-198.

(93)   Pal, D.; Chakrabarti, P. On residues in the disallowed region of the Ramachandran map. *Biopolymers* **2002**, *63*, 195-206.

(94)   Shoemaker, K. R.; Kim, P. S.; York, E. J.; Stewart, J. M.; Baldwin, R. L. Tests of the Helix Dipole Model for Stabilization of Alpha-Helices. *Nature* **1987**, *326*, 563-567.

(95)   Frisch, M. J.; Trucks, G. W.; Schlegel, H. B.; Scuseria, G. E.; Robb, M. A.; Cheeseman, J. R.; Scalmani, G.; Barone, V.; Mennucci, B.; Petersson, G. A.; Nakatsuji, H.; Caricato, M.; Li, X.; Hratchian, H. P.; Izmaylov, A. F.; Bloino, J.; Zheng, G.; Sonnenberg, J. L.; Hada, M.; Ehara, M.; Toyota, K.; Fukuda, R.; Hasegawa, J.; Ishida, M.; Nakajima, T.; Honda, Y.; Kitao, O.; Nakai, H.; Vreven, T.; Montgomery, J., J. A.; Peralta, J. E.; Ogliaro, F.; Bearpark, M.; Heyd, J. J.; Brothers, E.; Kudin, K. N.; Staroverov, V. N.; Keith, T.; Kobayashi, R.; Normand, J.; Raghavachari, K.; Rendell, A.; Burant, J. C.; Iyengar, S. S.; Tomasi, J.; Cossi, M.; Rega, N.; Millam, J. M.; Klene, M.; Knox, J. E.; Cross, J. B.; Bakken, V.; Adamo, C.; Jaramillo, J.; Gomperts, R.; Stratmann, R. E.; Yazyev, O.; Austin, A. J.; Cammi, R.; Pomelli, C.; Ochterski,

J. W.; Martin, R. L.; Morokuma, K.; Zakrzewski, V. G.; Voth, G. A.; Salvador, P.; Dannenberg, J. J.; Dapprich, S.; Daniels, A. D.; Farkas, O.; Foresman, J. B.; Ortiz, J. V.; Cioslowski, J.; Fox, D. J.: Gaussian 09, Revision D.01. Gaussian, Inc.: Wallingford, CT, 2013.

(96)   Tomasi, J.; Mennucci, B.; Cances, E. The IEF version of the PCM solvation method: an overview of a new method addressed to study molecular solutes at the QM ab initio level. *J. Mol. Struct. THEOCHEM* **1999**, *464*, 211-226.

(97)   Dunning, T. H., Jr. Gaussian basis sets for use in correlated molecular calculations: The atoms boron through neon and hydrogen. *J. Chem. Phys.* **1989**, *90*, 1007-1023.

(98)   Boys, S. F.; Bernardi, F. Calculation of Small Molecular Interactions by Differences of Separate Total Energies - Some Procedures with Reduced Errors. *Mol. Phys.* **1970**, *19*, 553-566.

(99)   Simon, S.; Duran, M.; Dannenberg, J. J. How does basis set superposition error change the potential surfaces for hydrogen bonded dimers? *J. Chem. Phys.* **1996**, *105*, 11024-11031.

(100)   Peverati, R.; Truhlar, D. G. M11-L: A Local Density Functional That Provides Improved Accuracy for Electronic Structure Calculations in Chemistry and Physics. *J. Chem. Phys. Lett.* **2012**, *3*, 117-124.

(101)   Weigend, F.; Ahlrichs, R. Balanced basis sets of split valence, triple zeta valence and quadruple zeta valence quality for H to Rn: Design and assessment of accuracy. *Phys. Chem. Chem. Phys.* **2005**, *7*, 3297-3305.

(102)   Men, L.; Wang, Y. S. Further studies on the fragmentation of protonated ions of peptides containing aspartic acid, glutamic acid, cysteine sulfinic acid, and cysteine sulfonic acid. *Rapid Commun. Mass. Spec.* **2005**, *19*, 23-30.